A high-order implicit finite element method for integrating the two-fluid magnetohydrodynamic equations in two dimensions

S.C. Jardin *, J. Breslau, N. Ferraro

Plasma Physics Laboratory, Princeton University, P.O. Box 451, Princeton, NJ 08543-451, United States

Abstract

We describe a new method for solving the time-dependent two-fluid magnetohydrodynamic (2F-MHD) equations in two dimensions that has significant advantages over other methods. The stream-function/potential representation of the velocity and magnetic field vectors, while fully general, allows accurate description of nearly incompressible fluid motions and manifestly satisfies the divergence condition on the magnetic field. Through analytic manipulation, the split semi-implicit method breaks the full matrix time advance into four sequential time advances, each involving smaller matrices. The use of a high-order triangular element with continuous first derivatives (C^1 continuity) allows the Galerkin method to be applied without introduction of new auxiliary variables (such as the vorticity or the current density). These features, along with the manifestly compact nature of the fully node-based C^1 finite elements, lead to minimum size matrices for an unconditionally stable method with order of accuracy h^4. The resulting matrices are compatible with direct factorization using SuperLU_dist. We demonstrate the accuracy of the method by presenting examples of two-fluid linear wave propagation, two-fluid linear eigenmodes of a tilting cylinder, and of a challenging nonlinear problem in two-fluid magnetic reconnection.
© 2007 Elsevier Inc. All rights reserved.

1. Introduction

It is well known that the "two-fluid" magnetohydrodynamic (2F-MHD) equations for a magnetized plasma present many numerical challenges. Even in the simpler ideal MHD model, a symmetric hyperbolic system which is a subset of the 2F-MHD equations, there are three distinct wave types with a wide separation of propagation speeds and with complex polarizations when applied to magnetized plasma conditions typical of fusion plasmas. When discretized on a finite difference or finite element mesh, these alone lead to a range of timescales and accuracy requirements that are a challenge to address with a single simulation [1].

---

* Corresponding author. Tel.: +1 609 243 2635; fax: +1 609 243 2662.
  E-mail address: jardin@pppl.gov (S.C. Jardin).

The full 2F-MHD equations compound this difficulty by introducing new terms which add dissipative phenomena and wave dispersion into the system [2]. Fully explicit solution techniques for 2F-MHD are generally not practical for magnetic fusion applications except for simulating the fastest timescale phenomena, which is of limited interest. To address the slower timescales, an implicit method is required, and the multiple-time-scales and differing polarizations then manifest themselves as one or more poorly conditioned matrix equations that need to be solved to advance the solution from one timestep to the next. These matrices are either calculated analytically [3–5] (as in this paper) or are formed numerically as part of a nonlinear Newton method [6–8].

It has been shown that in two dimensions (2D), a particular 18 degree-of-freedom polynomial triangular finite element with C^1 continuity, sometimes called the "reduced quintic" or Q_{18}, offers some unique advantages over other representations [9–11]. This element represents each scalar field in each triangular element as a quintic polynomial, which would normally require 21 coefficients. Of these, 18 are determined by the data (six values at each node: the value of the function and its first and second derivatives) and the other three by the requirement that the normal derivative along each edge be a cubic polynomial in the edge length, from which the C^1 property follows. The resulting representation contains a complete quartic polynomial, and thus has leading error of order h^5. It is also fully bivariate, and thus free of the directional bias that a tensor product representation would introduce.

The Q_{18} element has the fewest number of degrees-of-freedom (DOF) compared to other finite elements representations with the same asymptotic error, and thus leads to implicit matrix equations of minimum rank [3]. This follows from the fact that all the DOF are defined at the nodes, and are thus shared by all the surrounding triangular elements. Also, the C^1 continuity property allows these elements to be applied directly to equations with spatial derivatives of up to fourth-order by using the Galerkin method and shifting two of the derivatives to the trial function by integration by parts. This makes feasible the numerical solution of the 2F-MHD equations in their stream function/potential form, which has many advantages over solving the primitive form of the equations, especially when a strong background magnetic field is present.

The work presented here is a continuation and generalization of Appendix D of Ref. [3]. In that work, a method was presented for the 2-field reduced MHD equations in 2D slab geometry. This has subsequently been generalized to the 4-field Fitzpatrick-Porcelli equations [4]. In the present work, we generalize these equations to the "complete" 8-field two-fluid model, but continue to restrict the geometry to 2D slab geometry. One feature of this formulation is that the previous 2-field and four-field models will be seen to be non-trivial subsets of the more complete model presented here. This allows direct comparison with and evaluation of the assumptions made in developing the reduced models.

2. The equations

Consider the set of 2F-MHD equations [20] for the evolution of the plasma number density, the mass-flow velocity, the ion pressure, the electron pressure and the magnetic field, and the definitions of the electric field and the electrical current density (in SI units):

$$\frac{\partial n}{\partial t} + \nabla \cdot (n\vec{V}) = 0 \tag{2.1a}$$

$$nM_i\left(\frac{\partial \vec{V}}{\partial t} + \vec{V} \cdot \nabla \vec{V}\right) + \nabla p = \vec{J} \times \vec{B} + M_i n\vec{g} - \nabla \cdot \overleftrightarrow{\Pi}_i \tag{2.1b}$$

$$\frac{1}{(\gamma-1)}\left[\frac{\partial p_i}{\partial t} + \nabla \cdot (p_i\vec{V})\right] = -p_i\nabla \cdot \vec{V} - \overleftrightarrow{\Pi}_i : \nabla \vec{V} - \nabla \cdot \vec{q}_i - Q_\Delta \tag{2.1c}$$

$$\frac{1}{(\gamma-1)}\left[\frac{\partial p_e}{\partial t} + \nabla \cdot (p_e\vec{V})\right] = -p_e\nabla \cdot \vec{V} + \frac{\vec{J}}{ne} \cdot \left[\frac{n^\gamma}{(\gamma-1)}\nabla(p_e/n^\gamma) + \vec{R}\right] + \nabla\left(\frac{\vec{J}}{ne}\right) : \overleftrightarrow{\Pi}_e - \nabla \cdot \vec{q}_e + Q_\Delta \tag{2.1d}$$

$$\frac{\partial \vec{B}}{\partial t} = -\nabla \times \vec{E} \tag{2.1e}$$

$$\vec{E} + \vec{V} \times \vec{B} = \frac{1}{ne}(\vec{R} + \vec{J} \times \vec{B} - \nabla p_e - \nabla \cdot \overset{\leftrightarrow}{\Pi}_e) \tag{2.1f}$$

$$\mu_0 \vec{J} = \nabla \times \vec{B} \tag{2.1g}$$

Here, the random heat flux vectors for the ions and electrons are denoted $\vec{q}_i$ and $\vec{q}_e$, the equipartition term is denoted $Q_\Delta \equiv 3m_e(p - 2p_e)/(M_i\tau_e)$, and we have introduced the ratio of specific heats, γ, which has the classical value of $\gamma = 5/3$. The electron–ion momentum transfer term is taken here to have the simplified form proportional to the plasma current; $\vec{R} = \eta ne\vec{J}$ although future studies will use the more correct form $\vec{R} = \eta ne\left(\vec{J} + \frac{3e}{5T_e}\vec{q}_e\right)$. A gravitational force $\vec{g} \equiv -g\hat{y}$ has been included, where g is a constant. The last two equations imply that the total fluid pressure, denoted by $p \equiv p_e + p_i$, obeys the equation:

$$\frac{1}{(\gamma-1)}\left[\frac{\partial p}{\partial t} + \nabla \cdot (p\vec{V})\right] = -p\nabla \cdot \vec{V} - \overset{\leftrightarrow}{\Pi}_i : \nabla\vec{V} - \nabla \cdot (\vec{q}_i + \vec{q}_e)$$

$$+ \frac{\vec{J}}{ne} \cdot \left[\frac{n^\gamma}{(\gamma-1)}\nabla(p_e/n^\gamma) + \vec{R}\right] + \nabla\left(\frac{\vec{J}}{ne}\right) : \overset{\leftrightarrow}{\Pi}_e \tag{2.2}$$

These equations have the energy integral:

$$\frac{\partial}{\partial t}\left[\frac{1}{2\mu_0}B^2 + \frac{1}{2\mu_0}nM_iV^2 + \frac{p}{(\gamma-1)}\right]$$

$$= -\nabla \cdot \left[\frac{\gamma}{(\gamma-1)}\left(p\vec{V} - \frac{p_e\vec{J}}{en}\right) + \vec{E} \times \vec{B} + \overset{\leftrightarrow}{\Pi}_i \cdot \vec{V} - \frac{1}{ne}\overset{\leftrightarrow}{\Pi}_e \cdot \vec{J} + \frac{1}{2}nM_iV^2\vec{V} + \vec{q}_e + \vec{q}_i\right] + M_in\vec{V} \cdot \vec{g} \tag{2.3}$$

This implies conservation of energy if the gravitational potential is absent and the flux terms on the right vanish everywhere on the computational boundary.

The ion viscous stress term is taken to have the form:

$$\overset{\leftrightarrow}{\Pi}_i = -\mu[\nabla\vec{V} + \nabla\vec{V}^\dagger] - 2(\mu_C - \mu)(\nabla \cdot \vec{V})\overset{\leftrightarrow}{I} + \overset{\leftrightarrow}{\Pi}_i^{GV}$$

$$\nabla \cdot \overset{\leftrightarrow}{\Pi}_i = -\mu\nabla^2\vec{V} - (2\mu_C - \mu)\nabla(\nabla \cdot \vec{V}) + \nabla \cdot \overset{\leftrightarrow}{\Pi}_i^{GV} \tag{2.4}$$

Here μ and μ_C are the incompressible and compressible coefficients of viscosity that satisfy the positivity constraints $\mu > 0$ and $\mu_C > (2/3)\mu$ [12]. In the present work, we are not including the gyroviscous contribution (the rightmost term) in Eq. (2.4) in either the formulation or the examples. The inclusion of this term is discussed in [13].

We take the electron stress tensor to have the form of a hyper-resistivity, with coefficient λ:

$$\overset{\leftrightarrow}{\Pi}_e = \lambda\eta ne\nabla\vec{J} \tag{2.5}$$

The heat flux terms are expressed in terms of the isotropic and parallel heat flux coefficients $\kappa^e, \kappa, \kappa_\parallel^e$, and $\kappa_\parallel$. They have the following form:

$$\vec{q} = -\kappa\nabla T - \kappa_\parallel\nabla_\parallel T$$

$$\vec{q}_e = -\kappa^e\nabla T_e - \kappa_\parallel^e\nabla_\parallel T_e \tag{2.6}$$

The incorporation of the parallel heat flux terms is discussed in [3] and for that reason will not be repeated in the formulation presented here. The temperatures are defined in terms of the pressures and densities as

$$T_e = \frac{p_e}{k_B n}, \quad T = \frac{p}{k_B n}, \tag{2.7}$$

In the remainder of the paper we adopt the normalized form of the equations. The normalization amounts to adopting a standard density and magnetic field strength n_0 and B_0. All lengths, velocities, and pressures are then scaled to the ion skin depth, the Alfven velocity, and the magnetic pressure in the usual way:

$$l_0 \equiv \frac{c}{\omega_{pi}} = \left[\frac{M_i}{n_0 e^2 \mu_0}\right]^{1/2}$$

$$V_0 \equiv \frac{B_0}{\sqrt{\mu_0 M_i n_0}} \tag{2.8}$$

$$p_0 = \frac{B_0^2}{\mu_0}$$

Other scaled quantities can be derived from these using dimensional relations. For example the time is scaled to $t_0 = l_0/V_0$, etc.

3. The numerical representation

In 2D (x, y plane), without loss of generality, we represent the fluid velocity and magnetic field in terms of the five scalar variables $U(x,y,t), \chi(x,y,t), V_z(x,y,t), \psi(x,y,t), I(x,y,t)$ as follows:

$$\vec{V} = \nabla U \times \hat{z} + \nabla \chi + V_z \hat{z},$$
$$\vec{B} = \nabla \psi \times \hat{z} + I\hat{z} \tag{3.1}$$

This representation, which is the Cartesian limit of that used in the M3D code [14], effectively separates incompressible and compressible motions in order to minimize spectral pollution [1]. Also, the form for the magnetic field is intrinsically divergence-free and involves only two scalar variables.

Each of the scalar variables is expanded in a set of polynomial triangular finite elements. At each node, there are 6 degrees-of-freedom (DOF) for each scalar, corresponding to the value of the function and its 2 first and 3 second derivatives at that node. Basis functions $v_i(x,y)$ are chosen that are piecewise quintic with the property that the function and its first derivative are continuous across element boundaries. Each basis function has the value of unity for one of the six DOF for that function at one node, with the property that the basis function and its two first and three second derivatives vanish at all the surrounding nodes as described in [3].

Within each triangular finite element, the solution is expressed as the sum of the product of the 18 time-independent spatial basis functions for that element, $v_j(x,y)$, (six from each of the three nodes) times the time-dependent amplitudes. Thus, for example, at time $t = t^n$, the velocity stream function in a particular triangular element is represented as

$$U(x,y,t^n) = \sum_{j=1}^{18} U_j^n v_j(x,y) \tag{3.2}$$

In a similar way, the other seven scalar fields $\chi, V_z, \psi, I, n, p, p_e$ at time t^n are represented by the amplitudes: $X_j^n, V_{zj}^n, \Psi_j^n, I_j^n, N_j^n, P_j^n, P_{ej}^n$. To derive the discrete form of the velocity advance equations, we first operate on the momentum equation (2.1b) with the three annihilation operators

$$-\hat{z} \cdot \nabla \times$$
$$\hat{z}\cdot \tag{3.3}$$
$$\nabla\cdot$$

These have the effect of removing the compressible motion from the first equation, and the incompressible motion from the third. To form the weak form of the equations as required by the Galerkin method, each equation is then multiplied by each basis function $v_i(x,y)$ (six for each node) and then integrated over the domain. Integration by parts converts the three annihilation operators in (3.3) to the vector projections:

$$\hat{z} \cdot \nabla v_i \times$$
$$v_i \hat{z}\cdot \tag{3.3$'$}$$
$$-\nabla v_i\cdot$$

The integration by parts that was performed here and in the following introduces boundary terms. Each of these boundary terms will contain v_i and/or its normal derivative. We use the property of the basis functions, described previously, that only one basis function for each scalar variable is non-zero at a given boundary point, and only one other has a non-zero normal derivative. We apply homogeneous Dirichlet and/or Neumann boundary conditions by replacing the row in the matrix that corresponds to multiplying by these basis functions by a row with all zeros except a one on the diagonal, and by a zero on the right side of the equals sign. This effectively removes these basis functions from the representation at the boundary, in effect creating an essential boundary condition there, and thus the corresponding boundary term vanishes.

Straightforward manipulation, neglecting terms involving spatial derivatives of the viscosities and of the density multiplying the viscosities, and using Stokes and Gauss's theorems to convert total derivatives to boundary terms that vanish, yields the following integral equations for the weak form of the three scalar momentum equations. For each test function $v_i(x, y)$, we have

$$\int\int \left\{ \begin{array}{l} -n(v_i, \dot{U}) + n[v_i, \dot{\chi}] - n\nabla^2 U[v_i, U] + \frac{1}{2}n[v_i, (U, U)] - n\nabla^2 U(v_i, \chi) \\ +[n, v_i][\chi, U] + \frac{1}{2}n[v_i, (\chi, \chi)] + \nabla^2\psi[v_i, \psi] - gv_i n_x - \mu\nabla^2 v_i \nabla^2 U \end{array} \right\} dx\,dy = 0 \tag{3.4}$$

$$\int\int \left\{ v_i n\dot{V}_z + v_i n[V_z, U] + v_i n(V_z, \chi) + \mu\nabla v_i \cdot \nabla V_z + v_i[\psi, I] \right\} dx\,dy = 0 \tag{3.5}$$

$$\int\int \left\{ \begin{array}{l} -n[v_i, \dot{U}] - n(v_i, \dot{\chi}) + n\nabla^2 U(v_i, U) - \frac{1}{2}n(v_i, (U, U)) - n\nabla^2 U[v_i, \chi] \\ -n(v_i, [\chi, U]) - \frac{1}{2}n(v_i, (\chi, \chi)) - \nabla^2\psi(v_i, \psi) + gv_i n_y - 2\mu_C\nabla^2 v_i\nabla^2\chi \\ -I(v_i, I) - (v_i, p) \end{array} \right\} dx\,dy = 0 \tag{3.6}$$

Here and elsewhere we use the notation that for any two scalar quantities a and b, we define the Poisson bracket: $[a, b] \equiv \hat{z} \cdot \nabla a \times \nabla b = a_x b_y - a_y b_x$, and the inner product of the gradients: $(a, b) \equiv \nabla a \cdot \nabla b = a_x b_x + a_y b_y$, where subscripts here denote partial differentiation. Also, time derivatives have been denoted with a dot: i.e. $\dot{U} \equiv \partial U/\partial t$.

Next consider the field equations. Substitution of Eq. (3.1) into Eqs. (2.1a), (2.1d), and (2.2) yields

$$\dot{n} + [n, U] + (n, \chi) + n\nabla^2\chi = 0 \tag{3.7}$$

$$\dot{p}_e + [p_e, U] + (p_e, \chi) + \gamma p_e \nabla^2\chi = S_{pe} \tag{3.8}$$

$$\dot{p} + [p, U] + (p, \chi) + \gamma p\nabla^2\chi = S_\kappa + S_P \tag{3.9}$$

The magnetic field evolution equation (2.1e), together with the Generalized Ohm's law (2.1f) yield, upon substitution:

$$\dot{\psi} + [\psi, U] + (\psi, \chi) = S_\psi \tag{3.10}$$

$$\dot{I} + [I, U] + (I, \chi) + I\nabla^2\chi + [\psi, V_z] = S_I \tag{3.11}$$

Here, we have defined the effective source terms:

$$S_\kappa \equiv (\gamma - 1)\nabla \cdot [\kappa\nabla(p/n)]$$

$$S_p \equiv \frac{1}{n}[p_e, I] - \gamma\frac{p_e}{n^2}[n, I] + (\gamma - 1)\left[\begin{array}{l} \eta(|\nabla^2\psi|^2 + |\nabla I|^2) \\ +\lambda\eta(|\nabla(\nabla^2\psi)|^2 + I_{xx}^2 + I_{yy}^2 + 2I_{xy}^2) \end{array} \right]$$
$$+ (\gamma - 1)\left[\begin{array}{l} \mu[(\chi_{xx} - \chi_{yy} + 2U_{xy})^2 + (U_{yy} - U_{xx} + 2\chi_{xy})^2] \\ +(2\mu_C - \mu)|\nabla^2\chi|^2 + \mu(V_z, V_z) \end{array} \right] \tag{3.12}$$

$$S_{pe} \equiv \frac{1}{n}[p_e, I] - \gamma\frac{p_e}{n^2}[n, I] + (\gamma - 1)\left[\begin{array}{l} \nabla \cdot \kappa_e\nabla(p_e/n) + \eta(|\nabla^2\psi|^2 + |\nabla I|^2) \\ +\lambda\eta(|\nabla(\nabla^2\psi)|^2 + I_{xx}^2 + I_{yy}^2 + 2I_{xy}^2) + \alpha(p - 2p_e) \end{array} \right] \tag{3.13}$$

$$S_\psi \equiv \eta(\nabla^2\psi - \lambda\nabla^4\psi) + d_i n^{-1}[\psi, I] \tag{3.14}$$

$$S_I \equiv \eta(\nabla^2 I - \lambda\nabla^4 I) + d_i n^{-1}[\nabla^2\psi, \psi] + d_i\nabla^2\psi[n^{-1}, \psi] + d_i I[n^{-1}, I] + d_i[n^{-1}, p_e] \tag{3.15}$$

Note that we have neglected (assumed small) terms proportional to the gradients of η, μ, μ_C, and of λ, and have introduced the inverse equi-partition time: $\alpha \equiv 3m_e/(M_i\tau_e)$. The parameter d_i that appears in the source terms (3.14) and (3.15) is equal to unity for the standard normalization given in Eq. (2.8), but is included so that we can easily change the ion skin depth without changing other problem parameters or dimensions. When present, the scale length is $l_0 \equiv c/(d_i\omega_{pi})$.

4. The implicit time advance equations for the velocity variables

The implicit time advance we use is similar to that described in [5,21]. For illustration, it is applied to a simple wave equation in Appendix C. It is based on the fact that the ideal MHD wave characteristics are contained in both the velocity advance and the field advance equations. In order to combine these into a single, higher order equation for efficient implicit solution, we introduce the implicitness parameter $0 < \theta < 1$ and use this to evaluate the velocity variables in the field evolution equations (3.7) and (3.9)–(3.11) at an advanced time for substitution into the momentum equations. Thus, Taylor expanding the velocity variables in these equations about the present time t^n to evaluate at time $t^n + \theta\delta t$ yields

$$\dot{n} + [n, U + \theta\delta t\dot{U}] + (n, \chi + \theta\delta t\dot{\chi}) + n\nabla^2(\chi + \theta\delta t\dot{\chi}) = 0 \tag{4.1}$$

$$\dot{p} + [p, U + \theta\delta t\dot{U}] + (p, \chi + \theta\delta t\dot{\chi}) + \gamma p\nabla^2(\chi + \theta\delta t\dot{\chi}) = S_\kappa + S_p \tag{4.2}$$

$$\dot{\psi} + [\psi, U + \theta\delta t\dot{U}] + (\psi, \chi + \theta\delta t\dot{\chi}) = S_\psi \tag{4.3}$$

$$\dot{I} + [I, U + \theta\delta t\dot{U}] + (I, \chi + \theta\delta t\dot{\chi}) + I(\nabla^2\chi + \theta\delta t\nabla^2\dot{\chi}) + [\psi, V_z + \theta\delta t\dot{V}_z] = S_I \tag{4.4}$$

Consider now the weak form of the first momentum equation (3.4). Similarly Taylor expanding the velocity and field variables in time, again using the implicitness parameter θ, and substituting in from the field equations (4.1)–(4.4) for the time derivatives of the field variables that appear, gives the implicit form of the first velocity equation that we use. Thus for each test function $v_i(x, y)$, we have the integral equation:

$$\int\int I_i\,\mathrm{d}x\,\mathrm{d}y = 0 \tag{4.5a}$$

Where the integrand is given by

$$
I_i = \left\{
\begin{array}{l}
-n(v_i, \dot{U}) + n[v_i, \dot{\chi}] - n\nabla^2 U[v_i, U] + \frac{1}{2}n[v_i, (U, U)] - n\nabla^2 U(v_i, \chi) \\
+ [n, v_i][\chi, U] + \frac{1}{2}n[v_i, (\chi, \chi)] + \nabla^2\psi[v_i, \psi] - gv_i n_x - \mu\nabla^2 v_i\nabla^2 U
\end{array}
\right\}
$$
$$
+ \theta\delta t\left\{
\begin{array}{l}
-n\nabla^2\dot{U}[v_i, U] - n\nabla^2 U[v_i, \dot{U}] + n[v_i, (U, \dot{U})] + n[v_i, (\chi, \dot{\chi})] \\
-n\nabla^2\dot{U}(v_i, \chi) - n\nabla^2 U(v_i, \dot{\chi}) + [n, v_i][\dot{\chi}, U] + [n, v_i][\chi, \dot{U}] \\
-\mu\nabla^2 v_i\nabla^2\dot{U}
\end{array}
\right\}
$$
$$
+ \theta\delta t\left\{
\begin{array}{l}
([\psi, U], [v_i, \psi]) + ((\psi, \chi), [v_i, \psi]) - \nabla^2\psi[v_i, [\psi, U]] \\
-\nabla^2\psi[v_i, (\psi, \chi)] + gv_{ix}[n, U] + gv_{ix}(n, \chi) + gv_{ix}n\nabla^2\chi \\
-(S_\psi, [v_i, \psi]) + \nabla^2\psi[v_i, S_\psi]
\end{array}
\right\}
$$
$$
+ (\theta\delta t)^2\left\{
\begin{array}{l}
([\psi, \dot{U}], [v_i, \psi]) + ((\psi, \dot{\chi}), [v_i, \psi]) - \nabla^2\psi[v_i, [\psi, \dot{U}]] \\
-\nabla^2\psi[v_i, (\psi, \dot{\chi})] + gv_{ix}[n, \dot{U}] + gv_{ix}(n, \dot{\chi}) + gv_{ix}n\nabla^2\dot{\chi}
\end{array}
\right\} \tag{4.5b}
$$

Note that since the purpose of this was to make implicit the convective terms and the wave motion, the density needed to be expanded only when it multiplied the gravitational term. As explained in Appendix C, the resulting velocity equations are in a form that will lead to a method that is second-order accurate in time (for $\theta = 1/2$), and can be time advanced to the new time level without further coupling to the field variables. We next note that the terms in Eq. (4.5) that involve the field source terms S_ψ are small for fusion applications and can be omitted in the velocity advance equations (although they are retained in the field equation advance). This

formally leads to an error of order δt, but with a very small coefficient. We find that omitting these terms improves the nonlinear stability of the method without a noticeable effect on the accuracy.

We observe that the time derivatives of two of the velocity variables, $\dot{U}$ and $\dot{\chi}$, appear in many places at this stage. Next, expanding all the scalar variables as in Eq. (3.2) and integrating over the domain, we make use of the definitions in Appendix A to rewrite Eq. (4.5) as the system of discrete equations:

$$G_{i,j,k}^2 N_k \dot{U}_j + K_{i,j,k} N_k \dot{X}_j + V_{i,j,k,l}^1 N_l U_k U_j + V_{i,j,k,l}^3 N_l X_k U_j + V_{i,j,k,l}^5 N_l X_k X_j - G_{i,j,k} \Psi_j \Psi_k + g X_{i,j}^0 N_j$$

$$+ \mu G_{i,j,k}^3 U_j N_k + \theta \delta t \left\{ \begin{array}{l} V_{i,j,k,l}^1 N_l [\dot{U}_k U_j + U_k \dot{U}_j] + V_{i,j,k,l}^3 N_l [\dot{X}_k U_j + \dot{X}_k \dot{U}_j] \\ + V_{i,j,k,l}^5 N_l [\dot{X}_k X_j + X_k \dot{X}_j] + \mu G_{i,j,k}^3 \dot{U}_j N_k \end{array} \right\}$$

$$+ \theta \delta t \{ C_{i,j,k,l}^1 \Psi_k \Psi_l U_j + C_{i,j,k,l}^3 \Psi_k \Psi_l X_j + g [X_{i,j,k}^1 N_k U_j + X_{i,j,k}^2 N_k X_j] \} + (\theta \delta t)^2 \{ C_{i,j,k,l}^1 \Psi_k \Psi_l \dot{U}_j$$

$$+ C_{i,j,k,l}^3 \Psi_k \Psi_l \dot{X}_j + g [X_{i,j,k}^1 N_k \dot{U}_j + X_{i,j,k}^2 N_k \dot{X}_j] \} = 0 \tag{4.6}$$

Summation over repeated indices is implied. We next multiply by the time step, δt, and finite difference in time, centering the time derivatives about time $t = (n + 1/2)\delta t$, so that $\delta t \dot{U}_j = [U_j^{n+1} - U_j^n]$, etc. In order to enable strictly linear calculations, we express all state variables as the sum of a time independent equilibrium part and a time varying perturbed part; i.e. $U_j^n \to U_j^0 + U_j^n$, etc. (Note that this is just done to enable the possibility of linear calculations about an equilibrium state and this split does not affect the nonlinear calculations.) We can then put Eq. (4.6) in the form

$$S_{11}^v U^{n+1} + S_{12}^v V_z^{n+1} + S_{13}^v X^{n+1} = D_{11}^v U^n + D_{12}^v V_z^n + D_{13}^v X^n + R_{11}^v \Psi^n + R_{12}^v I^n + R_{13}^v P^n + O_1^v \tag{4.7}$$

Here, the block matrix elements are defined as

$$S_{11}^v U^{n+1} = \left\{ \begin{array}{l} N_k G_{i,j,k}^2 + \theta \delta t [-\mu B_{i,j} + N_l (V_{i,j,k,l}^1 + V_{i,j,k,l}^2)(U_k + U_k^0) + N_l V_{i,j,k,l}^3 (X_k + X_k^0)] \\ + \theta^2 \delta t^2 [C_{i,j,k,l}^1 (\Psi_l + \Psi_l^0)(\Psi_k + \Psi_k^0) + g X_{i,j,k}^1 N_k] \end{array} \right\} U_j^{n+1}$$

$$S_{12}^v V_z^{n+1} = 0$$

$$S_{13}^v X^{n+1} = \left\{ \begin{array}{l} N_k K_{i,j,k} + \theta \delta t N_l [(U_k + U_k^0) V_{i,j,k,l}^4 + (V_{i,j,k,l}^5 + V_{i,j,k,l}^6)(X_k + X_k^0)] \\ + \theta^2 \delta t^2 [C_{i,j,k,l}^3 (\Psi_l + \Psi_l^0)(\Psi_k + \Psi_k^0) + g X_{i,j,k}^2 N_k] \end{array} \right\} X_j^{n+1}$$

$$D_{11}^v U^n = \left\{ \begin{array}{l} N_k G_{i,j,k}^2 + \delta t \left(\begin{array}{l} (1 - \theta)\mu B_{i,j} + (V_{i,j,k,l}^1 + V_{i,j,k,l}^2) N_l [\theta(U_k + U_k^0) - (\frac{1}{2} U_k + U_k^0)] \\ + V_{i,j,k,l}^3 N_l [\theta(X_k + X_k^0) - (\frac{1}{2} X_k + X_k^0)] \end{array} \right) \\ + \theta(\theta - 1)\delta t^2 [C_{i,j,k,l}^1 (\Psi_l + \Psi_l^0)(\Psi_k + \Psi_k^0) + g X_{i,j,k}^1 N_k] \end{array} \right\} U_j^n$$

$$D_{12}^v V_z^n = 0$$

$$D_{13}^v X^n = \left\{ \begin{array}{l} N_k K_{i,j,k} + \delta t N_l \left(\begin{array}{l} V_{i,j,k,l}^4 [\theta(U_k + U_k^0) - (\frac{1}{2} U_k + U_k^0)] \\ (V_{i,j,k,l}^5 + V_{i,j,k,l}^6)[\theta(X_k + X_k^0) - (\frac{1}{2} X_k + X_k^0)] \end{array} \right) \\ + \theta(\theta - 1)\delta t^2 [C_{i,j,k,l}^3 (\Psi_l + \Psi_l^0)(\Psi_k + \Psi_k^0) + g X_{i,j,k}^2 N_k] \end{array} \right\} X_j^n$$

$$R_{11}^v \Psi^n = \left\{ \begin{array}{l} \delta t (\frac{1}{2} \Psi_k + \Psi_k^0)(G_{i,j,k} + G_{i,k,j}) \\ - \theta \delta t^2 [(C_{i,k,l,j}^3 + C_{i,k,j,l}^3) X_k^0 + (C_{i,k,j,l}^1 + C_{i,k,l,j}^1) U_k^0](\frac{1}{2} \Psi_l + \Psi_l^0) \end{array} \right\} \Psi_j^n$$

$$R_{12}^v I^n = 0$$

$$R_{13}^v P^n = 0$$

$$O_1^v = \delta t g X_{i,j}^0 N_j$$

A similar procedure is applied to the second and third momentum equation. We make use of the definitions in Appendix A to define the additional block matrix elements:

$$S_{21}^v U^{n+1} = \left\{ \theta\delta t N_l V_{i,j,k,l}^8 (V_{zk}^n + V_{zk}^0) - (\theta\delta t)^2 C_{i,j,k,l}^5 (\Psi_k + \Psi_k^0)(I_l + I_l^0) \right\} U_j^{n+1}$$

$$S_{22}^v V_z^{n+1} = \left\{ \begin{array}{l} N_k K_{i,j,k}^1 + \theta\delta t \left[-\mu(A_{i,j} - hB_{i,j}) + N_l V_{i,j,k,l}^7 (U_k + U_k^0) + V_{i,j,k,l}^9 N_l(X_k + X_k^0) \right] \\ -\theta^2 \delta t^2 C_{i,j,k,l}^9 (\Psi_k + \Psi_k^0)(\Psi_l + \Psi_l^0) \end{array} \right\} V_{zj}^{n+1}$$

$$S_{23}^v X^{n+1} = \{ \theta\delta t N_l V_{i,j,k,l}^{10}(V_{zk}^n + V_{zk}^0) - (\theta\delta t)^2 C_{i,j,k,l}^7 (\Psi_k + \Psi_k^0)(I_l + I_l^0) \} X_j^{n+1}$$

$$D_{21}^v U^n = \left\{ \delta t V_{i,j,k,l}^8 N_l \left[\theta(V_{zk}^n + V_{zk}^0) - (\tfrac{1}{2} V_{zk}^n + V_{zk}^0) \right] - \theta(\theta-1)\delta t^2 C_{i,j,k,l}^5 (\Psi_k + \Psi_k^0)(I_l + I_l^0) \right\} U_j^n$$

$$D_{22}^v V_z^n = \left\{ K_{i,j,k}^1 N_k + \delta t \left(\begin{array}{l} (1-\theta)\mu(A_{i,j} - hB_{i,j}) + N_l V_{i,j,k,l}^7 \left[\theta(U_k + U_k^0) - (\tfrac{1}{2} U_k + U_k^0) \right] \\ + N_l V_{i,j,k,l}^9 \left[\theta(X_k + X_k^0) - (\tfrac{1}{2} X_k + X_k^0) \right] \\ -\theta(\theta-1)\delta t^2 C_{i,j,k,l}^9 (\Psi_k + \Psi_k^0)(\Psi_l + \Psi_l^0) \end{array} \right) \right\} V_{zj}^n$$

$$D_{23}^v X^n = \left\{ \delta t V_{i,j,k,l}^{10} N_l \left[\theta(V_{zk}^n + V_{zk}^0) - (\tfrac{1}{2} V_{zk}^n + V_{zk}^0) \right] - \theta(\theta-1)\delta t^2 C_{i,j,k,l}^7 (\Psi_k + \Psi_k^0)(I_l + I_l^0) \right\} X_j^n$$

$$R_{21}^v \psi^n = \left\{ -\delta t K_{i,j,k}(\tfrac{1}{2} I_k + I_k^0) + \theta\delta t^2 \left[\begin{array}{l} (C_{i,k,j,l}^5 U_l^0 + C_{i,k,j,l}^7 X_l^0)(\tfrac{1}{2} I_l + I_l^0) \\ (C_{i,k,j,l}^9 + C_{i,k,l,j}^9)(\tfrac{1}{2} \Psi_l + \Psi_l^0) V_k^0 \end{array} \right] \right\} \Psi_j$$

$$R_{22}^v I^n = \left\{ -\delta t K_{i,k,j}(\tfrac{1}{2} \Psi_k + \Psi_k^0) + \theta\delta t^2 \left[(C_{i,l,k,j}^5 U_l^0 + C_{i,l,k,j}^7 X_l^0)(\tfrac{1}{2} \Psi_k + \Psi_k^0) \right] \right\} I_j$$

$$R_{23}^v P^n = 0$$

$$O_2^v = \theta\delta t^2 C_{i,j,k,l}^9 \Psi_l^0 \Psi_k^0 V_j^0$$

$$S_{31}^v U^{n+1} = \left\{ \begin{array}{l} -K_{i,j,k} N_k + \theta\delta t N_l [V_{i,j,k,l}^{12}(X_k + X_k^0) + (V_{i,j,k,l}^{16} + V_{i,j,k,l}^{15})(U_k + U_k^0)] \\ + (\theta\delta t)^2 \left[\begin{array}{l} C_{i,j,k,l}^{11}(\Psi_k + \Psi_k^0)(\Psi_l + \Psi_l^0) + C_{i,j,k,l}^{15}(I_k + I_k^0)(I_l + I_l^0) \\ -G_{i,j,k}^7(P_k + P_k^0) - g Y_{i,j,k}^1 N_k \end{array} \right] \end{array} \right\} U_j^{n+1}$$

$$S_{32}^v V_z^{n+1} = (\theta\delta t)^2 C_{i,j,k,l}^{15}(\Psi_k + \Psi_k^0)(I_l + I_l^0) V_l^{n+1}$$

$$S_{33}^v X^{n+1} = \left\{ \begin{array}{l} G_{i,j,k}^2 N_k + \theta\delta t [-2\mu_C B_{i,j} + N_l V_{i,j,k,l}^{11}(U_k + U_k^0) + N_l(V_{i,j,k,l}^{13} + V_{i,j,k,l}^{14})(X_k + X_k^0)] \\ + (\theta\delta t)^2 \left[\begin{array}{l} C_{i,j,k,l}^{13}(\Psi_k + \Psi_k^0)(\Psi_l + \Psi_l^0) + C_{i,j,k,l}^{17}(I_k + I_k^0)(I_l + I_l^0) \\ -(G_{i,j,k}^{6A} + \gamma G_{i,j,k}^{6B})(P_k + P_k^0) - g Y_{i,j,k}^2 N_k + C_{i,j,k,l}^{17} I_l^{0SI} I_k^{0SI} \end{array} \right] \end{array} \right\} X_j^{n+1}$$

$$D_{31}^v U^n = \left\{ \begin{array}{l} -K_{i,j,k} N_k + \delta t N_l \left[\begin{array}{l} V_{i,j,k,l}^{12}[\theta(X_k + X_k^0) - (\tfrac{1}{2} X_k + X_k^0)] \\ + (V_{i,j,k,l}^{15} + V_{i,j,k,l}^{16})[\theta(U_k + U_k^0) - (\tfrac{1}{2} U_k + U_k^0)] \end{array} \right] \\ +\theta(\theta-1)\delta t^2 \left[\begin{array}{l} C_{i,j,k,l}^{11}(\Psi_k + \Psi_k^0)(\Psi_l + \Psi_l^0) + C_{i,j,k,l}^{15}(I_k + I_k^0)(I_l + I_l^0) \\ -G_{i,j,k}^7(P_k + P_k^0) - g Y_{i,j,k}^1 N_k \end{array} \right] \end{array} \right\} U_j^n$$

$$D_{32}^v V_z^n = \theta(\theta-1)\delta t^2 C_{i,j,k,l}^{15}(\Psi_k + \Psi_k^0)(I_l + I_l^0) V_j^n$$

$$D_{33}^v X^n = \left\{ \begin{array}{l} G_{i,j,k}^2 N_k + \delta t \left[\begin{array}{l} (1-\theta)2\mu_C B_{i,j} + N_l V_{i,j,k,l}^{11}[\theta(U_k + U_k^0) - (\tfrac{1}{2} U_k + U_k^0)] \\ + N_l(V_{i,j,k,l}^{13} + V_{i,j,k,l}^{14})[\theta(X_k + X_k^0) - (\tfrac{1}{2} X_k + X_k^0)] \end{array} \right] \\ +\theta(\theta-1)\delta t^2 \left[\begin{array}{l} C_{i,j,k,l}^{13}(\Psi_k + \Psi_k^0)(\Psi_l + \Psi_l^0) + C_{i,j,k,l}^{17}(I_k + I_k^0)(I_l + I_l^0) \\ -(G_{i,j,k}^{6A} + \gamma G_{i,j,k}^{6B})(P_k + P_k^0) - g Y_{i,j,k}^2 N_k \end{array} \right] \\ +(\theta\delta t)^2 C_{i,j,k,l}^{17} I_k^{0SI} I_l^{0SI} \end{array} \right\} X_j^n$$

$$R_{31}^v \Psi^n = \left\{ \begin{array}{l} \delta t[G_{i,k,j}^4 + G_{i,j,k}^4](\tfrac{1}{2} \Psi_k + \Psi_k^0) \\ -\theta\delta t^2 \left[\begin{array}{l} ([C_{i,k,j,l}^{11} + C_{i,k,l,j}^{11}]U_l^0 + [C_{i,k,j,l}^{13} + C_{i,k,l,j}^{13}]X_k^0)(\tfrac{1}{2} \Psi_l + \Psi_l^0) \\ + C_{i,k,j,l}^{15} V_k^0(\tfrac{1}{2} I_l + I_l^0) \end{array} \right] \end{array} \right\} \Psi_j$$

$$R_{32}^v I^n = \left\{ \begin{array}{l} \delta t \left[G_{i,k,j}^5 + G_{i,j,k}^5 \right](\tfrac{1}{2} I_k + I_k^0) \\ -\theta\delta t^2 \left[\begin{array}{l} ([C_{i,k,j,l}^{15} + C_{i,k,l,j}^{15}]U_k^0 + [C_{i,k,j,l}^{17} + C_{i,k,l,j}^{17}]X_k^0)(\tfrac{1}{2} I_l + I_l^0) \\ + C_{i,l,k,j}^{15} V_l^0(\tfrac{1}{2} \Psi_k + \Psi_k^0) \end{array} \right] \end{array} \right\} I_j$$

$$R_{33}^v P^n = \{ -\delta t A_{i,j} + \theta\delta t^2 [G_{i,k,j}^7 U_k^0 + G_{i,k,j}^6 X_k^0] \} P_j$$

$$O_v^3 = -\theta\delta t^2 C_{i,j,k,l}^{15} V_j^0 \Psi_k^0 I_l^0 - \delta t g Y_{i,j}^0 N_j$$

Here we have introduced a variable for the reciprocal of the density: $1/n = \sum_{j=1}^{18} v_j E_j$.

With these definitions, the three momentum equations are combined into the single block matrix equation:

$$
\begin{bmatrix} S_{11}^v & S_{12}^v & S_{13}^v \\ S_{21}^v & S_{22}^v & S_{23}^v \\ S_{31}^v & S_{32}^v & S_{33}^v \end{bmatrix} \cdot \begin{bmatrix} U \\ V_z \\ X \end{bmatrix}^{n+1} = \begin{bmatrix} D_{11}^v & D_{12}^v & D_{13}^v \\ D_{21}^v & D_{22}^v & D_{23}^v \\ D_{31}^v & D_{32}^v & D_{33}^v \end{bmatrix} \cdot \begin{bmatrix} U \\ V_z \\ X \end{bmatrix}^{n} + \begin{bmatrix} R_{11}^v & R_{12}^v & R_{13}^v \\ R_{21}^v & R_{22}^v & R_{23}^v \\ R_{31}^v & R_{32}^v & R_{33}^v \end{bmatrix} \begin{bmatrix} \psi \\ I \\ P \end{bmatrix}^{n} + \begin{bmatrix} O_1^v \\ O_2^v \\ O_3^v \end{bmatrix} \quad (4.15)
$$

It is one of the major features of this method that only the old time values of the field variables appear in Eq. (4.15), so that the implicit coupling is only between the velocity variables. Thus, the analytic manipulation has led to a compact implicit equation which contains within it all of the MHD wave characteristics. By factoring the matrix on the left and solving this system, we are able to take time steps that are not limited by the Courant condition based on the MHD waves in the system or by any diffusive phenomena. We note here that Eq. (4.15) has two important sub-systems that can be solved in a fraction of the run time of the full system. Keeping only the terms in the upper left corners in the three matrices gives the two-field reduced MHD system considered in [3]. Keeping only the upper left 2×2 sub-blocks gives the four-field system discussed in [4]. These reduced systems are valuable for both debugging the full system, and for better understanding the incremental physical effects that the full system introduces.

5. The implicit field equations

Once the velocity variables are updated to the new time, the density equation can be updated independent of the other field equations. Again, using the implicitness parameter θ to evaluate quantities at the advanced time, we define the matrix elements:

$$S_{11}^n N_j^{n+1} = \{D_{i,j} + \theta \delta t [K_{i,j,k}(U_k + U_k^0) + G_{i,k,j}^2 (X_k + X_k^0)]\} N_j^{n+1}$$

$$D_{11}^n N_j^n = \left\{ \begin{array}{l} D_{i,j} + \delta t K_{i,j,k}[\theta(U_k + U_k^0) - (\tfrac{1}{2}U_k^n + U_k^0)] \\ \quad + \delta t G_{i,k,j}^2 [\theta(X_k + X_k^0) - (\tfrac{1}{2}X_k^n + X_k^0)] \end{array} \right\} N_j^n$$

$$R_{11}^n U_j^{n+1} = -\theta \delta t K_{i,k,j}(N_k + N_k^0) U_j^{n+1}$$

$$R_{12}^n = 0$$

$$R_{13}^n X_j^{n+1} = -\theta \delta t G_{i,j,k}^2 (N_k + N_k^0) X_j^{n+1}$$

$$Q_{11}^n U_j^n = -\delta t K_{i,k,j}\left[(\tfrac{1}{2}N_k^n + N_k^0) - \theta(N_k + N_k^0) \right] U_j^n$$

$$Q_{12}^n = 0$$

$$Q_{13}^n X_j^n = -\delta t G_{i,j,k}^2 \left[(\tfrac{1}{2}N_k^n + N_k^0) - \theta(N_k + N_k^0) \right] X_j^n$$

These allow us to write the implicit density advance as a block matrix equation:

$$
S_{11}^n \cdot N^{n+1} = D_{11}^n \cdot N^n + [R_{11}^n \quad R_{12}^n \quad R_{13}^n] \cdot \begin{bmatrix} U \\ V_z \\ X \end{bmatrix}^{n+1} + [Q_{11}^n \quad Q_{12}^n \quad Q_{13}^n] \cdot \begin{bmatrix} U \\ V_z \\ X \end{bmatrix}^{n} \quad (5.1)
$$

In a similar way, for the pressure advance we define the block matrix elements:

$$S_{11}^p P_j^{n+1} = \left\{ \begin{array}{l} D_{i,j} + \theta \delta t K_{i,j,k}(U_k + U_k^0) \\ \quad - \theta \delta t (\gamma - 1)\kappa (G_{i,j,k} + G_{i,k,j}) E_k \\ \quad + \theta \delta t [G_{i,k,j}^2 - (\gamma - 1)K_{i,k,j}^2](X_k + X_k^0) \end{array} \right\} P_j^{n+1}$$

$$D_{11}^p P_j^n = \left\{ \begin{array}{l} D_{i,j} + \delta t K_{i,j,k}\left[\theta(U_k + U_k^0) - \left(\frac{1}{2}U_k^n + U_k^0\right)\right] \\ + (1 - \theta)\delta t(\gamma - 1)\kappa(G_{i,j,k} + G_{i,k,j})E_k \\ + \delta t[G_{i,k,j}^2 - (\gamma - 1)K_{i,j,k}^2]\left[\theta(X_k + X_k^0) - \left(\frac{1}{2}X_k^n + X_k^0\right)\right] \end{array} \right\} P_j^n$$

$$R_{11}^p U_j^{n+1} = -\theta\delta t K_{i,k,j}(P_k + P_k^0)U_j^{n+1}$$

$$R_{12}^p = 0$$

$$R_{13}^p X_j^{n+1} = -\theta\delta t[G_{i,j,k}^2 - (\gamma - 1)K_{i,j,k}^2](P_k + P_k^0)X_j^{n+1}$$

$$Q_{11}^p U_j^n = -\delta t K_{i,k,j}\left[\left(\frac{1}{2}P_k^n + P_k^0\right) - \theta(P_k + P_k^0)\right]U_j^n$$

$$Q_{12}^p = 0$$

$$Q_{13}^p X_j^n = -\delta t[G_{i,j,k}^2 - (\gamma - 1)K_{i,j,k}^2]\left[\left(\frac{1}{2}P_k + P_k^0\right) - \theta(P_k + P_k^0)\right]X_j^n$$

$$O_1^p = \delta t[D_{i,j}S_{pj} + (\gamma - 1)\kappa(G_{i,k,j}^2 + G_{i,j,k}^2 - h_p G_{i,k,j}^{13})E_k P_j^0]$$

Using these, the pressure equation can be written as

$$S_{11}^p \cdot P^{n+1} = D_{11}^p \cdot P^n + \begin{bmatrix} R_{11}^p & R_{12}^p & R_{13}^p \end{bmatrix} \cdot \begin{bmatrix} U \\ V_z \\ X \end{bmatrix}^{n+1} + \begin{bmatrix} Q_{11}^p & Q_{12}^p & Q_{13}^p \end{bmatrix} \cdot \begin{bmatrix} U \\ V_z \\ X \end{bmatrix}^n + O_1^p \qquad (5.2)$$

Next, consider the remaining field equations for the two components of the magnetic field and for the electron pressure. These are solved simultaneously in order to capture the coupling that leads to the Whistler and kinetic Alfven modifications to the MHD waves. Thus, in a similar manner, we form a set of implicit equations for the field and electron pressure variables by Taylor expanding all variables in time and keeping the terms linear in δt. Applying the Galerkin method and making use of the definitions in Appendix A yields the following block matrix form for these remaining time advance equations:

$$\begin{bmatrix} S_{11}^b & S_{12}^b & S_{13}^b \\ S_{21}^b & S_{22}^b & S_{23}^b \\ S_{31}^b & S_{32}^b & S_{33}^b \end{bmatrix} \cdot \begin{bmatrix} \psi \\ I \\ P_e \end{bmatrix}^{n+1} = \begin{bmatrix} D_{11}^b & D_{12}^b & D_{13}^b \\ D_{21}^b & D_{22}^b & D_{23}^b \\ D_{31}^b & D_{32}^b & D_{33}^b \end{bmatrix} \cdot \begin{bmatrix} \psi \\ I \\ P_e \end{bmatrix}^n + \begin{bmatrix} R_{11}^b & R_{12}^b & R_{13}^b \\ R_{21}^b & R_{22}^b & R_{23}^b \\ R_{31}^b & R_{32}^b & R_{33}^b \end{bmatrix} \cdot \begin{bmatrix} U \\ V_z \\ X \end{bmatrix}^{n+1}$$

$$+ \begin{bmatrix} Q_{11}^b & Q_{12}^b & Q_{13}^b \\ Q_{21}^b & Q_{22}^b & Q_{23}^b \\ Q_{31}^b & Q_{32}^b & Q_{33}^b \end{bmatrix} \cdot \begin{bmatrix} U \\ V_z \\ X \end{bmatrix}^n + \begin{bmatrix} O_1 \\ O_2 \\ O_3 \end{bmatrix} \qquad (5.3)$$

The matrix elements are defined as follows:

$$S_{11}^b \Psi_j^{n+1} = \left\{ D_{i,j} + \theta\delta t \begin{bmatrix} K_{i,j,k}(U_k + U_k^0) - \eta(A_{i,j} - \lambda B_{i,j}) \\ -G_{j,k,i}^2(X_k + X_k^0) - d_i U_{i,j,k,l}^3 E_l(I_k + I_k^0) \end{bmatrix} \right\} \Psi_j^{n+1}$$

$$S_{12}^b I_j^{n+1} = -\theta\delta t d_i U_{i,j,k,l}^4 E_l(\Psi_k + \Psi_k^0)I_j^{n+1}$$

$$S_{13}^b = 0$$

$$D_{11}^b \Psi_j^n = \left\{ \begin{array}{l} D_{i,j} + \delta t K_{i,j,k}\left[\theta(U_k + U_k^0) - \left(\frac{1}{2}U_k + U_k^0\right)\right] + (\theta - 1)\delta t\eta(A_{i,j} - \lambda B_{i,j}) \\ -\delta t G_{j,k,i}^2\left[\theta(X_k + X_k^0) - \left(\frac{1}{2}X_k + X_k^0\right)\right] - \delta t d_i U_{i,j,k,l}^3 E_l\left[\theta(I_k + I_k^0) - \left(\frac{1}{2}I_k + I_k^0\right)\right] \end{array} \right\} \Psi_j^n$$

$$D_{12}^b I_j = -\left\{ \delta t d_i U_{i,j,k,l}^4 E_l\left[\theta(\Psi_k + \Psi_k^0) - \left(\frac{1}{2}\Psi_k + \Psi_k^0\right)\right] \right\} I_j$$

$$D_{13}^b = 0$$

$$R_{11}^b U_j^{n+1} = -\theta\delta t K_{i,k,j}(\Psi_k + \Psi_k^0)U_j^{n+1}$$

$$R_{12}^b = 0$$

$$R_{13}^b X_j^{n+1} = \theta \delta t G_{k,j,i}^2 (\Psi_k + \Psi_k^0) X_j^{n+1}$$

$$O_1 = \delta t [\eta(A_{i,j} - \lambda B_{i,j}) \Psi_j^0 + d_i U_{i,j,k,l}^3 E_l \Psi_j^0 I_k^0]$$

$$Q_{11}^b U_j^n = \delta t K_{i,k,j} [\theta(\Psi_k + \Psi_k^0) - (\tfrac{1}{2}\Psi_k + \Psi_k^0)] U_j^n$$

$$Q_{12}^b = 0$$

$$Q_{13}^b X_j^n = -\delta t G_{k,j,i}^2 [\theta(\Psi_k + \Psi_k^0) - (\tfrac{1}{2}\Psi_k + \Psi_k^0)] X_j^n$$

$$S_{21}^b \Psi_j^{n+1} = \theta \delta t \Big\{ K_{i,j,k}(V_{zk} + V_{zk}^0) - d_i(U_{i,j,k,l}^1 + U_{i,j,k,l}^2) E_l(\Psi_k + \Psi_k^0) \Big\} \Psi_j^{n+1}$$

$$S_{22}^b I_j^{n+1} = \left[D_{i,j} + \theta \delta t \begin{pmatrix} -\eta(A_{i,j} - \lambda B_{i,j}) + K_{i,j,k}(U_k + U_k^0) \\ + G_{i,k,j}^2 (X_k + X_k^0) - d_i(U_{i,j,k,l}^5 + U_{i,j,k,l}^6)(I_k + I_k^0)E_l \end{pmatrix} \right] I_j^{n+1}$$

$$S_{23}^b P_{ej}^{n+1} = -\theta \delta t d_i K_{i,k,j} E_k P_{ej}^{n+1}$$

$$D_{21}^b \Psi_j^n = \delta t \Big\{ K_{i,j,k}[\theta(V_{zk} + V_{zk}^0) - (\tfrac{1}{2}V_{zk} + V_{zk}^0)] - d_i(U_{i,j,k,l}^1 + U_{i,j,k,l}^2)E_l[\theta(\Psi_k + \Psi_k^0) - (\tfrac{1}{2}\Psi_k + \Psi_k^0)] \Big\} \Psi_j^n$$

$$D_{22}^b I_j^n = \left\{ \begin{array}{l} D_{i,j} - (\theta-1)\delta t \eta(A_{i,j}\eta_k - \lambda B_{i,j}) + \delta t K_{i,j,k}[\theta(U_k + U_k^0) - (\tfrac{1}{2}U_k + U_k^0)] \\ + \delta t G_{i,k,j}^2[\theta(X_k + X_k^0) - (\tfrac{1}{2}X_k + X_k^0)] - \delta t d_i(U_{i,j,k,l}^5 + U_{i,j,k,l}^6)E_l[\theta(I_k + I_k^0) - (\tfrac{1}{2}I_k + I_k^0)] \end{array} \right\} I_j^n$$

$$D_{23}^b P_{ej}^n = (1-\theta)\delta t d_i K_{i,k,j} E_k P_{ej}^n$$

$$R_{21}^b U_j^{n+1} = -\theta \delta t K_{i,k,j}(I_k + I_k^0) U_j^{n+1}$$

$$R_{22}^b V_{zj}^{n+1} = -\theta \delta t K_{i,k,j}(\Psi_k + \Psi_k^0) V_{zj}^{n+1}$$

$$R_{23}^b X_j^{n+1} = -\theta \delta t G_{i,j,k}^2 (I_k + I_k^0) X_j^{n+1}$$

$$Q_{21}^b U_j^n = \delta t K_{i,k,j}[\theta(I_k + I_k^0) - (\tfrac{1}{2}I_k + I_k^0)] U_j^n$$

$$Q_{22}^b V_{zj}^n = \delta t K_{i,k,j}[\theta(\Psi_k + \Psi_k^0) - (\tfrac{1}{2}\Psi_k + \Psi_k^0)] V_{zj}^n$$

$$Q_{23}^b X_j^n = \delta t G_{i,j,k}^2[\theta(I_k + I_k^0) - (\tfrac{1}{2}I_k + I_k^0)] X_j^n$$

$$O_2 = \delta t \left[\begin{array}{l} \eta(A_{i,j} - \lambda B_{i,j})I_j^0 - K_{i,j,k}\Psi_j^0 V_k^0 \\ + d_i(U_{i,j,k,l}^1 E_l \Psi_j^0 \Psi_k^0 + U_{i,j,k,l}^3 E_j I_l^0 I_k^0 + K_{i,j,k}^0 E_j P_{ek}^0) \end{array} \right]$$

$$S_{31}^b = 0$$

$$S_{32}^b I_j^{n+1} = -\theta \delta t d_i(V_{i,j,k,l}^8 + \gamma U_{i,j,k,l}^6)(P_{ek} + P_{ek}^0)E_l I_j^{n+1}$$

$$S_{33}^b P_{ej}^{n+1} = \left\{ \begin{array}{l} D_{i,j}[1 + 2\delta t \theta(\gamma-1)\alpha] + \theta \delta t K_{i,j,k}(U_k + U_k^0) \\ -\theta \delta t d_i(V_{i,j,k,l}^7 + \gamma U_{i,j,k,l}^5)E_l(I_k + I_k^0) + \theta \delta t[G_{i,k,j}^2 - (\gamma-1)K_{i,k,j}^2](X_k + X_k^0) \\ -(\gamma-1)\theta \delta t \kappa[G_{i,k,j}^2 + G_{i,j,k}^2 - h_p G_{i,k,j}^{13}]N_k \end{array} \right\} P_{ej}^{n+1}$$

$$D_{31}^b = 0$$

$$D_{32}^b I_j^n = -\delta t d_i(V_{i,j,k,l}^8 + \gamma U_{i,j,k,l}^6)E_l[\theta(P_{ek} + P_{ek}^0) - (\tfrac{1}{2}P_{ek} + P_{ek}^0)]I_j^n$$

$$D_{33}^b P_{ej}^n = \left\{ \begin{array}{l} D_{i,j}[1 + 2\delta t(\theta-1)(\gamma-1)\alpha] + \delta t K_{i,j,k}[\theta(U_k + U_k^0) - (\tfrac{1}{2}U_k + U_k^0)] \\ -\delta t d_i(V_{i,j,k,l}^7 + \gamma U_{i,j,k,l}^5)[\theta(I_k + I_k^0) - (\tfrac{1}{2}I_k + I_k^0)]E_l \\ + \delta t[G_{i,k,j}^2 - (\gamma-1)K_{i,k,j}^2][\theta(X_k + X_k^0) - (\tfrac{1}{2}X_k + X_k^0)] \\ + (\gamma-1)(1-\theta)\delta t \kappa\{G_{k,j}^2 + G_{j,k}^2 - h_p G_{k,j}^{13}\}N_k \end{array} \right\} P_{ej}^n$$

$$R_{31}^b U_j^{n+1} = -\theta \delta t K_{i,k,j}(P_{ek} + P_{ek}^0) U_j^{n+1}$$

$$R_{32}^b = 0$$

$$R_{33}^b X_j^{n+1} = -\theta \delta t[G_{i,j,k}^2 - (\gamma-1)K_{i,j,k}^2](P_{ek} + P_{ek}^0) X_j^{n+1}$$

$$Q_{31}^b U_j^n = \delta t K_{i,k,j}[\theta(P_{ek} + P_{ek}^0) - (\tfrac{1}{2}P_{ek} + P_{ek}^0)] U_j^n$$

$$Q^b_{32} = 0$$

$$Q^b_{33}X^n_j = +\delta t\left[G^2_{i,j,k} - (\gamma - 1)K^2_{i,j,k}\right]\left[\theta(P_{ek} + P^0_{ek}) - (\tfrac{1}{2}P_{ek} + P^0_{ek})\right]X^n_j$$

$$O_3 = \delta t(\gamma - 1)\kappa[G^2_{i,k,j} + G^2_{i,j,k} - h_p G^{13}_{i,k,j}]E_k P^0_j + \delta t(V^7_{i,j,k,l} + \gamma U^5_{i,j,k,l})E_l I^0_k P^0_{ej}$$

$$\qquad + \delta t(\gamma - 1)\eta[(K^1_{i,j,k} - \lambda G^2_{k,j,i})(J_k + J^0_k)(J_j + J^0_j) + (-G^2_{k,j,i} + \lambda G^{12}_{i,j,k})(I_k + I^0_k)(I_j + I^0_j)]$$

$$\qquad + \delta t(\gamma - 1)\alpha D_{i,j} P_j$$

6. Smoothing of velocity fields, a semi-implicit operator, and well posedness

Here we describe three modifications to the previously described algorithm that serve to increase the robustness and nonlinear stability of the overall scheme.

The first is that we find it useful to incorporate a small "hyper-viscosity" term in the two momentum equations (3.4) and (3.6) in order to damp sub-element scale oscillations that might otherwise develop [22]. Since these terms would involve sixth-order derivatives of the U and χ fields, they cannot be straightforwardly incorporated into the time advance using elements with only C^1 continuity unless we introduce additional variables. We therefore introduce a time splitting where the scalar functions U and χ are first advanced without these terms, and then a "smoothing" step is applied where these operators are applied. Consider the split time advance for the vorticity. Let the time advance values at time level $(n + 1)$ but without these higher derivative operators applied be denoted by $(*)$. The advance from level $(*)$ to the new level $(n + 1)$ is given by

$$w^* = \nabla^2 U^*$$
$$\nabla^2 U^{n+1} = w^* - \delta t v_H[\theta \nabla^4 w^{n+1} + (1 - \theta)\nabla^4 w^*] \tag{6.1}$$
$$w^{n+1} = \nabla^2 U^{n+1}$$

Multiply through by each trial function v_i, and this is equivalent to the two equations:

$$D_{i,j}W^*_j = A_{i,j}U^*_j \tag{6.2a}$$

and

$$\begin{bmatrix} D_{i,j} & -A_{i,j} \\ \delta t v_H \theta B_{i,j} & A_{i,j} \end{bmatrix}\begin{bmatrix} W \\ U \end{bmatrix}^{n+1}_j = \begin{bmatrix} 0 \\ [D_{i,j} - \delta t v_H(1 - \theta)B_{i,j}]W^*_j \end{bmatrix} \tag{6.2b}$$

Since these matrices on the left do not change during the simulation (if the timestep and element geometry are constant), they can be factored at the initial time and the equations are then solved each timestep by an efficient back-substitution. In the examples in this paper, a hyper-viscosity was used with the value $v_H = h^2\mu$, where h is a typical triangle dimension and μ is the viscosity. Rerunning several cases with half this value had essentially no noticeable effect on the computed results.

A second modification is that it is sometimes useful to add a semi-implicit term to help stabilize the X equation. This is particularly true if the total magnetic field vanishes somewhere or is small at a point. To this end, we introduce an artificial "semi-implicit" magnetic field I^{0SI}_k and modify the matrix elements as follows:

$$S^v_{33} \to S^v_{33} + (\theta\delta t)^2 C^{17}_{i,j,k,l}(I^{0SI}_k)(I^{0SI}_l)$$
$$D^v_{33} \to D^v_{33} + (\theta\delta t)^2 C^{17}_{i,j,k,l}(I^{0SI}_k)(I^{0SI}_l) \tag{6.3}$$

This modification was not used in the examples presented in this paper.

A third technique has to do with the solubility condition on Eq. (3.6). Before being multiplied by the trial function and integrated by parts, this equation for the time derivative of the divergence of the velocity had the form:

$$\nabla \cdot n\nabla \dot{\chi} = r \quad \text{in the interior}$$
$$\frac{\partial \dot{\chi}}{\partial n} = 0 \quad \text{on the boundary}$$

(6.4)

It is well known that equations of this type have a solubility constraint that may not be exactly satisfied numerically, and are indeterminate in that if χ is a solution, then $\chi + c$ is also a solution for any constant c. To address both of these, we shift the spectrum by replacing the first of the equations in (6.4) with

$$(\nabla \cdot n\nabla - \varepsilon)\dot{\chi} = r$$

(6.5)

where ε is some small number typically 10^{-7} [15]. This is equivalent to adding a small positive definite term proportional to $\varepsilon\chi^2$ to the variational statement of Eq. (6.4) which will automatically seek the solution that minimizes $\varepsilon\chi^2$ as well as satisfies the differential equation.

7. Summary of the time advance

Here we summarize and discuss the time advance equations given in Section 6. Let us introduce the vectors $\mathbf{V^n}$, $\mathbf{N^n}$, $\mathbf{P^n}$, and $\mathbf{\Psi^n}$ that represent all the unknown degrees-of-freedom (DOF) that we are solving for. The velocity vector $\mathbf{V^n}$ contains the six DOF for each of the three scalar velocity variables (U, χ, V_z) at each grid point, the density vector $\mathbf{N^n}$ and the pressure vector $\mathbf{P^n}$ each contain 6 DOF at each grid point, and the field vector $\mathbf{\Psi^n}$ contains six DOF for each of the three scalar field variables (ψ, I, P_e) at each grid point. By defining the appropriate vector and matrix quantities, we can rewrite Eqs. (4.15), (5.1), (5.2) and (5.3) in the compact form:

$$\mathbf{S}^V \cdot \mathbf{V^{n+1}} = \mathbf{D}^V \cdot \mathbf{V^n} + \mathbf{R^V} \cdot \mathbf{\Psi^n} + \mathbf{O^V}$$

(7.1)

$$\mathbf{S}^N \cdot \mathbf{N^{n+1}} = \mathbf{D}^N \cdot \mathbf{N^n} + [\mathbf{R}^N]^\dagger \cdot \mathbf{V^{n+1}} + [\mathbf{Q}^N]^\dagger \cdot \mathbf{V^n} + \mathbf{O}^N$$

(7.2)

$$\mathbf{S}^P \cdot \mathbf{P^{n+1}} = \mathbf{D}^P \cdot \mathbf{P^n} + [\mathbf{R}^P]^\dagger \cdot \mathbf{V^{n+1}} + [\mathbf{Q}^P]^\dagger \cdot \mathbf{V^n} + \mathbf{O}^P$$

(7.3)

$$\mathbf{S}^B \cdot \mathbf{\Psi^{n+1}} = \mathbf{D}^B \cdot \mathbf{\Psi^n} + \mathbf{R}^B \cdot \mathbf{V^{n+1}} + \mathbf{Q}^B \cdot \mathbf{V^n} + \mathbf{O^B}$$

(7.4)

The matrices all contain the unknowns only at the old time level. Thru analytic manipulation, the split semi-implicit method has broken up the full implicit equations to these four separate smaller systems of equations.

The main computational work is in solving these matrix equations. If we have a grid system with M node points, then the matrices $\mathbf{S}^V$ and $\mathbf{S^B}$ are both sparse matrices of rank 18M, and the matrices $\mathbf{S}^N$ and $\mathbf{S}^P$ are sparse matrices of rank 6M. We use the parallel direct sparse solver, SuperLU_dist [19], and so the most computationally intensive part of the time advance is to factor these matrices. We note that the four matrices could be factored concurrently as there are no dependences (although this was not done in our examples). A typical run in Section 10 of 400 time-steps for the full eight-field system on a 121×121 grid point mesh required 13.2 h using two nodes (each with eight processors) on the NERSC IBM p575 Power 5 system (Bassi). We note that the timing is independent of the size of the time step since there are no iterations involved.

A model system that was amenable to stability analysis, but which has the essential features of (7.1) and (7.4), was shown to lead to an unconditionally stable numerical method for implicitness parameter $\theta > 1/2$ in [4]. We postulate that the full system presented here is also unconditionally stable for $\theta > 1/2$, and have observed this over a wide region in parameter space where we have used time steps δt many times the Courant condition based on any of the waves, and, of course, many times the explicit time step restriction associated with the diffusive terms. We choose the time step based on accuracy considerations alone.

What constitutes consistent and stable boundary conditions for a computational study of a two-fluid MHD plasma is still a subject of research. To circumvent this difficulty, we introduce a transition region where

the ion skin depth parameter d_i gets multiplied by a factor f that is unity in the interior and vanishes at the wall. Thus, if the computational domain extends from $0 < x < L_x$ and $0 < y < L_y$, we multiply d_i by the masking factor:

$$f = \frac{1}{2}\{1 + \tanh[-\alpha(r - r_0)]\}$$

In the examples presented in this paper $\alpha = 12, r_0 = 1.75$, and the normalized coordinate r is defined as follows:

$$r^2 = [(x - L_x/2)^2 + (y - L_y/2)^2]\frac{16}{L_xL_y} \quad \text{(non-periodic problem)}$$

$$r = |y - L_y/2|\frac{4}{L_y} \quad \text{(for problem periodic in x)}$$

The boundary conditions in the applications presented in the next three sections are thus appropriate for a $d_i = 0$ (resistive MHD) plasma. They are of two types: periodic or conducting-wall. Let $\hat{n}$ be a unit vector normal to the wall and $\hat{t} \equiv \hat{n} \times \hat{z}$ be a unit vector in the tangential direction. Dirichlet boundary conditions for all the perturbed field quantities are applied at the wall. For example, for the poloidal flux: $\psi = \psi_t = \psi_{tt} = 0$. The same is true for I, n, p_e, p, and for the z-component of the velocity, Vz. For the other velocity variables, we have for the stream function: $U = U_t = U_{tt} = U_{nn} = 0$, and for the potential: $\chi_n = \chi_{nt} = \chi_{nn} + \chi_{tt} = 0$.

8. Plane wave propagation

As a first test we examine the ability to calculate small amplitude wave propagation parallel to the poloidal field. Taking the density to be uniform and the electron pressure to vanish, we linearize about an equilibrium with $I = I_0, \psi = \delta y, p = p_0$, where $I_0 = 1, \delta = 0.1$, and $p_0 = 0.01$. This is meant to model the conditions in a low-beta tokamak plasma with propagation dominantly in the poloidal plane. In this case I corresponds to the toroidal field and ψ to the poloidal flux. Assuming sinusoidal variation in x and t: $\sin(kx - \omega t)$, we find the following dispersion relation for the square of the frequency, $\Omega = \omega^2$:

$$\begin{aligned}
&\Omega^3 + A\Omega^2 + B\Omega + C = 0 \\
&A = -k^2[2\delta^2 + \gamma p_0 + I_0^2 + k^2\delta^2] \\
&B = k^4[\delta^4 + \gamma p_0(2\delta^2 + k^2\delta^2) + \delta^2 I_0^2] \\
&C = -k^6 \gamma p_0 \delta^4
\end{aligned} \tag{8.1}$$

Here $\gamma = 5/3$ is the adiabatic index. For a particular value of $k = 1, 2, \ldots$, we define a doubly periodic domain with $0 < x < 2\pi/k$ and $0 < y < 2\pi/k$ and initialize the perturbation to be one of the three roots of Eq. (8.1) corresponding to the (i) Slow, (ii) Alfven, or (iii) Fast branch, modified by the two-fluid terms. We set $\psi = 10^{-4}$, and the other perturbed quantities are initialized as follows:

$$\begin{aligned}
&U = -(k/\omega)\delta\psi \\
&I = \left[\left(1 - \frac{k^2\delta^2}{\omega^2}\right) - \frac{I_0^2}{(\omega^2/k^2 - \gamma p_0)}\right]^{-1}(k^3/\omega)\delta\psi \\
&V = -(k/\omega)\delta I \\
&\chi = \frac{\omega I_0}{(\omega^2 - \gamma p_0 k^2)}I \\
&p = \gamma p_0(k^2/\omega)\chi
\end{aligned} \tag{8.2}$$

We follow the evolution of the wave for the time $T = 2\pi k/\omega$ that it should theoretically take to traverse a single period, and compute the L_2 norm of the difference between the final and initial conditions, normalized to the initial amplitude. In the computational studies, we included small dissipative terms with amplitude $\kappa = \mu = \eta = 4 \times 10^{-5}$ for the fast wave initialization and $\kappa = \mu = \eta = 4 \times 10^{-4}$ for the Alfven and Slow wave initializations. We note that this will affect the minimum value of the error that can be obtained as these are

not taken into account in the analytic dispersion relation. The layout of the triangular elements for the 4×4 case, and the initial 1D sinusoidal perturbation of the ψ function are shown in Fig. 1.

We plot the relative error in the plane wave convergence test for a particular wave number $k = 1$ in Fig. 2 as a function of the time step used in the calculation. The solid (black) curve was initialized to an eigenmode of the Fast Wave with $\omega/k = 1.018057$, the dashed (red) curve was initialized to the Alfven Wave with $\omega/k = 0.100329$, and the dotted (blue) curve was initialized to the Slow Wave with $\omega/k = 0.0126393$. For the Fast Wave we compute the L_2 error using the variable I, for the Alfven Wave we use ψ, and for the slow wave we use p. For the Fast wave we use an implicitness parameter of $\theta = 0.51$, and for the Alfven and Slow wave we used $\theta = 0.55$.
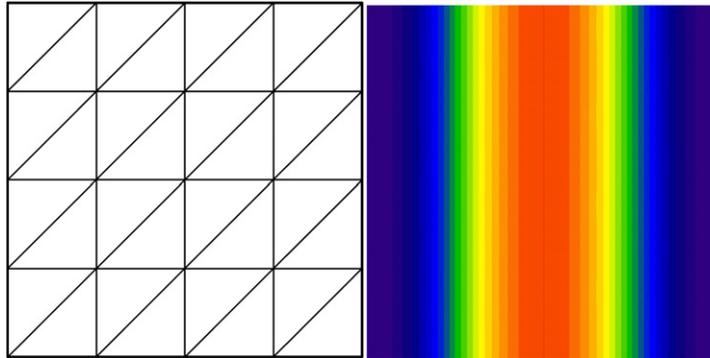
Fig. 1. Left shows arrangements of triangles for 4×4 doubly periodic wave propagation test. Right is corresponding initial contours of poloidal flux ψ.
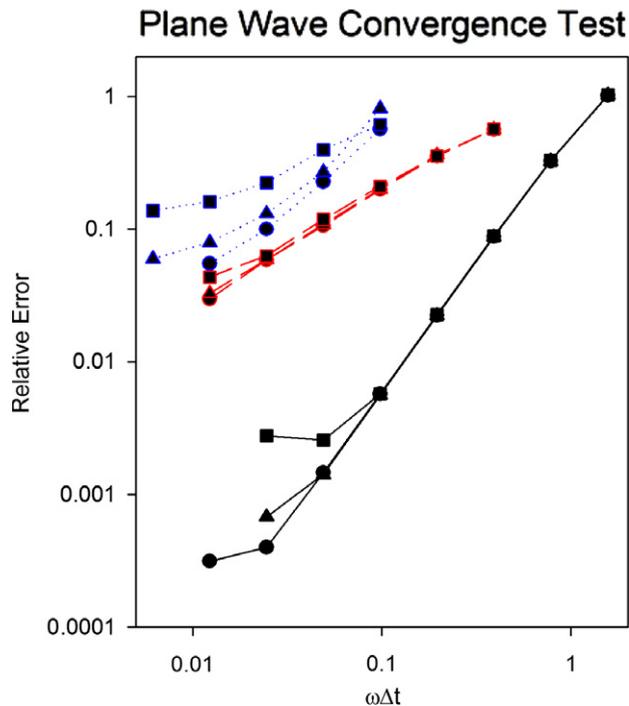
Fig. 2. Relative error after propagation for one wavelength when periodic plasma is initialized in an eigenmode of one of the three waves for wave number $k = 1$. The solid (black) curve was initialized to an eigenmode of the Fast Wave with $\omega/k = 1.018057$, the dashed (red) curve was initialized to the Alfven Wave with $\omega/k = 0.100329$, and the dotted (blue) curve was initialized to the Slow Wave with $\omega/k = 0.0126393$. Circles, triangles, and squares correspond to using 32, 8, and 4 triangles per linear wavelength.

This is a very stringent test as it measures to what degree the initial state is a "pure" eigenmode in both space and time. The total L_2 error is the result of many factors: the propagation velocity is slightly off, the wave damps, or other eigenmodes get excited. We can see that the Fast Wave is converging most rapidly as both the time step and mesh spacing decreases. The sub-dominant waves also are converging, but more slowly.

9. The tilting cylinder

This problem, in the resistive (single fluid) MHD limit, was proposed in [16], and solutions for reduced MHD are given in [3] (two-field model) and [4] (four-field model). Following [16], we define an initial bipolar vortex equilibrium state:

$$\psi^0(x,y) = \begin{cases} [2/kJ(k)]J_1(kr)\cos\theta, & r < 1 \\ (r - 1/r)\cos\theta, & r > 1 \end{cases} \quad J_1(k) = 0. \tag{9.1}$$

We have defined a polar coordinate system such that $y = r\cos\theta, x = r\sin\theta$. For given values of the parameters B_0 and β_P, the initial longitudinal field and electron pressure inside the radius $r < 1$ are defined as

$$[I^0(x,y)]^2 = B_0^2 + (1 - \beta_P)k^2[\psi^0(x,y)]^2$$
$$p_e^0(x,y) = \frac{1}{2}k^2\beta_P[\psi^0(x,y)]^2 + 0.01 \tag{9.2}$$

For $r > 1$, these are both constant so as to be continuous at $r = 1$. The initial ion pressure and density are set to zero and unity, respectively. In these calculations we took the background field $B_0 = 1$. It is readily verified that this specification corresponds to a configuration satisfying the equilibrium equation: $\nabla p = \vec{J} \times \vec{B}$.

To illustrate the flexibility of this approach, we have perturbed the above equilibrium and computed the time evolution for several sets of equilibrium parameters corresponding to varying the quantity β_P from zero to one, and varying the ion skin depth, to which the lengths are scaled. As an aid to doing this, we utilize the ion skin depth parameter d_i, discussed at the end of Section 3. This appears such that when $d_i = 1$ the ion skin depth is unity in these units, when $d_i = 0.1$, it is 1/10th unit, and when $d_i = 0$, the ion skin depth shrinks to zero and the equations reduce to resistive MHD. We compute the linear growth rate by renormalizing the solution back to a fixed amplitude each timestep N and computing the growth rate from the rate of change of the kinetic energy K^N: $\gamma = [K^{N+1} - K^N]/[\Delta t \times (K^{N+1} + K^N)]$. The values quoted are when this no longer changes with cycle number N. The normalizations used are those in Eq. (2.8).

The results of this study are shown in Figs. 3 and 4. The different curves in Fig. 3a correspond to different sets of equations, and β_P values of either zero or one. The curve $n = 1$ corresponds to just one velocity variable, U, and one field variable, ψ. The curve $n = 2$ adds the velocity variable V_z and the field variable I, and the curve $n = 3$ adds the velocity variable χ and the field variable p_e to give the full system of equations discussed in this paper. The curves corresponding to $n = 1$ and $n = 2$ were discussed in [3,4]. These were computed in our formulation by keeping just the upper left element and the upper 2×2 sub-matrix in our Eqs. (4.15) and (5.3). Fig. 3b presents a convergence study for one point, that with $\beta_P = 1, n = 3$, and $d_i = 0$. The growth rate is seen to converge very rapidly with the number of mesh points N and quadratic with the time step Δt.

We see from Fig. 3 that except for the $n = 1$ reduced model, the linear growth rate increases significantly as the ion skin depth becomes comparable to the equilibrium scale length. The $n = 2$ reduced model gives the correct qualitative behavior, but can be substantially off in the actual growth rate.

To illustrate the complexity of the linear eigenfunction and how it changes with the ion skin depth, we show five of the field variables and five of the velocity variables in Figs. 4a and 4b for several configurations corresponding to $\beta_P = 1$ and scanning several values of d_i. Note that only seven independent scalar variables are being integrated in time in this example (since the ion pressure is zero). While we have plotted the toroidal current density, the vorticity, and the velocity divergence, these are not independently time-advanced variables, but are obtained by taking the Laplacian of the poloidal flux ψ, the velocity stream function U, and the velocity potential χ, respectively.
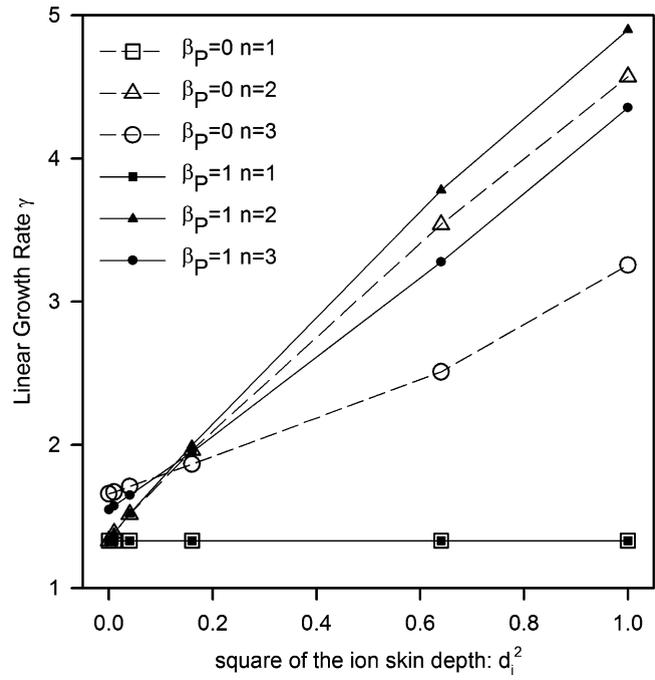
Fig. 3a. Growth rate vs ion skin depth for two equilibrium ($\beta_P = 0$ and $\beta_P = 1$) and for three sets of equations.
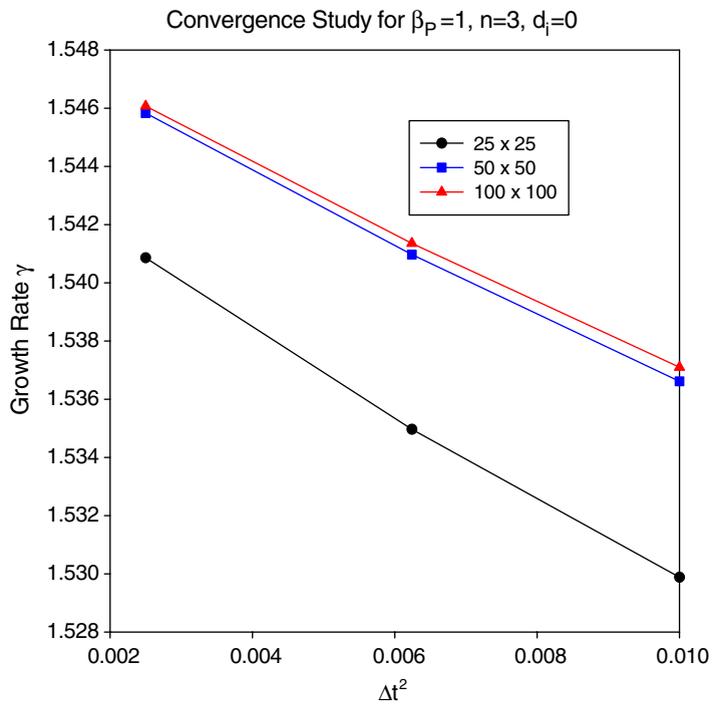

Fig. 3b. Convergence study for point in Fig. 3a with $\beta_P = 1$, $n = 3$, and $d_i = 0$. Shown are curves for 25×25, 50×50, and 100×100 mesh points in a rectangular domain.
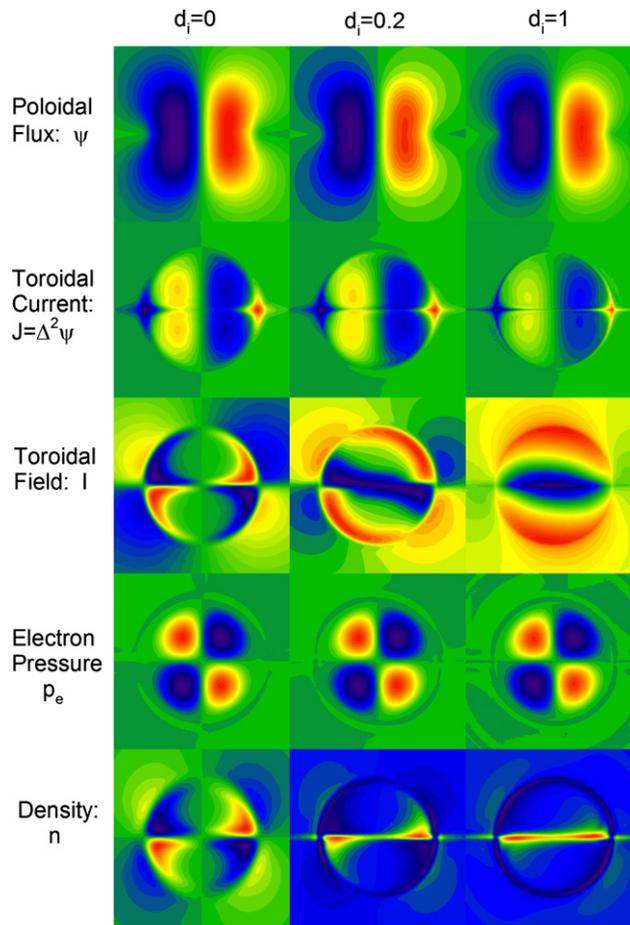
Fig. 4a. Linear eigenfunctions of the field variables for beta = 1 configurations for several values of d_i.

These growth rates were obtained using a uniformly laid-out triangular mesh such as shown in Fig. 1a. The baseline calculations were done with a mesh of 51×51 nodes and a timestep of $\Delta t = 0.05$. We find that the growth rates typically change only in the 4th decimal place when repeating the calculation on a mesh with 101×101 nodes, and in the 3rd decimal place when increasing the timestep to $\Delta t = 0.10$.

10. A reconnection problem

What has become a "standard problem" in two-fluid magnetic reconnection was proposed in [17]. We define an initial equilibrium as follows;

$$
\begin{aligned}
\psi^0(x,y) &= \frac{1}{2}\ln(\cosh 2y) \\
I^0(x,y) &= 0 \\
P^0(x,y) &= \frac{1}{2}[\operatorname{sech}^2(2y) + 0.2] \\
n^0(x,y) &= [\operatorname{sech}^2(2y) + 0.2] \\
P_e^0(x,y) &= 0.2 P^0(x,y)
\end{aligned}
\tag{10.1}
$$

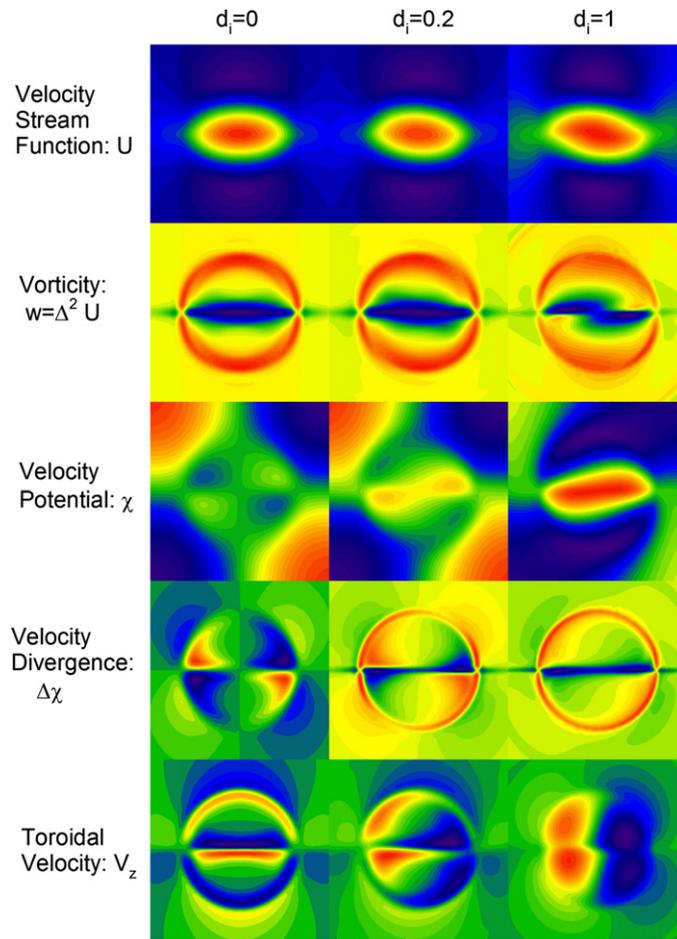All other quantities are initialized to zero. A perturbation is applied at time $t = 0$ as follows:

Fig. 4b. Linear eigenfunctions of the velocity variables for beta $= 1$ configurations for several values of d_i.

$$\psi(x,y) = \varepsilon \cos k_x x \cos k_y y. \tag{10.2}$$

The initial equilibrium and perturbed current densities are just the Laplacian of the fluxes, $J^0 = \nabla^2 \psi^0, J = \nabla^2 \psi$. The computation is carried out in a rectangular domain: $-L_x/2 \leqslant x \leqslant L_x/2$ and $-L_y/2 \leqslant y \leqslant L_y/2$. The system is taken to be periodic in the x-direction with ideal conducting boundaries at $y = \pm L_y/2$. The parameters are chosen such that $k_x = 2\pi/L_x, k_y = \pi/L_y$, with $L_x = 25.6, L_y = 12.8$, and $\varepsilon = 0.1$.

These calculations used values of resistivity $\eta = 0.005$, viscosities $\mu = \mu_C = 0.05$, and thermal conductivity $\kappa = 0.02$. An implicitness parameter of $\theta = 0.51$ was used. For all calculations presented, the time step used was as follows: From $t = 0$ to $t = 20$, $\Delta t = 0.2$; from $t = 20$ to $t = 24$, $\Delta t = 0.1$; from $t = 24$ to $t = 34$, $\Delta t = 0.05$; from $t = 34$ to $t = 40$, $\Delta t = 0.1$. These timesteps were chosen for accuracy considerations and were the same for all spatial resolutions. (We have verified that the calculation remains stable for arbitrarily large timestep, but the accuracy will deteriorate if the timestep is not lowered during periods of rapid change. A future timestep control algorithm will adjust the timestep automatically to retain adequate accuracy.) There were a total of 400 timesteps for each calculation.

We performed a series of calculations with $N \times N$ equally spaced nodes with $N = 61, 91, 121$, and 151. The triangular elements were then constructed by inserting diagonals similar to what is shown in Fig. 1. The inter-node spacing in the x-direction is denoted by Δx. This enters into the coefficients for the hyper-resistivity, Eq. (2.5), which we define as follows: $\lambda = C_H h^2$, where h is a typical triangle dimension and with the coefficient $C_H = 1.0$ used in these calculations. Since the physical value of the hyper-resistivity is smaller than any of
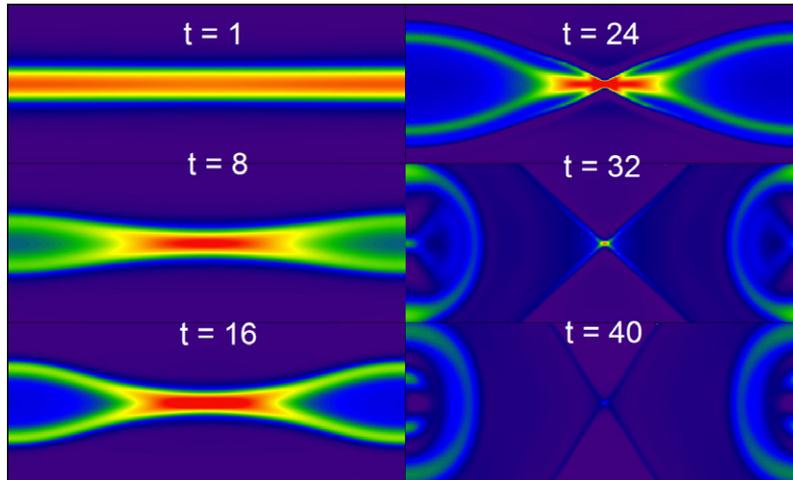
Fig. 5. Contours of the toroidal current density at selected times. Note that a transition occurs between the time of $t = 16$ and $t = 32$.

those used in this series, the meaningful result is to perform a convergence study and take the limit of $h \to 0$. The reason for choosing this dependency of λ on h is discussed below.

We show typical results for contours of the toroidal current density, $J = \nabla^2 \psi$, for the 121×121 nonlinear calculation at selected times in Fig. 5. We note that a transition occurs around the time $t = 24$, at which time the current density abruptly peaks on axis. To illustrate this more clearly, we show in Fig. 6 a plot of the current density along the $y = 0$ midplane as a function of the horizontal (x) distance and time. It can be seen from this graph how rapidly the transition occurs at time $t \sim 24$.

To understand this transition better, we plot in Fig. 7 the z-component of the electric field along the midplane, $y = 0$, at two times: $t = 20$ (before the transition) and $t = 30$ (after the transition). The total electric field is the smooth dark black line in Fig. 7. It is seen from Eq. (2.1f) that this is made up of several different contributions. For convenience, we rewrite the z-component of Eq. (2.1f) here:
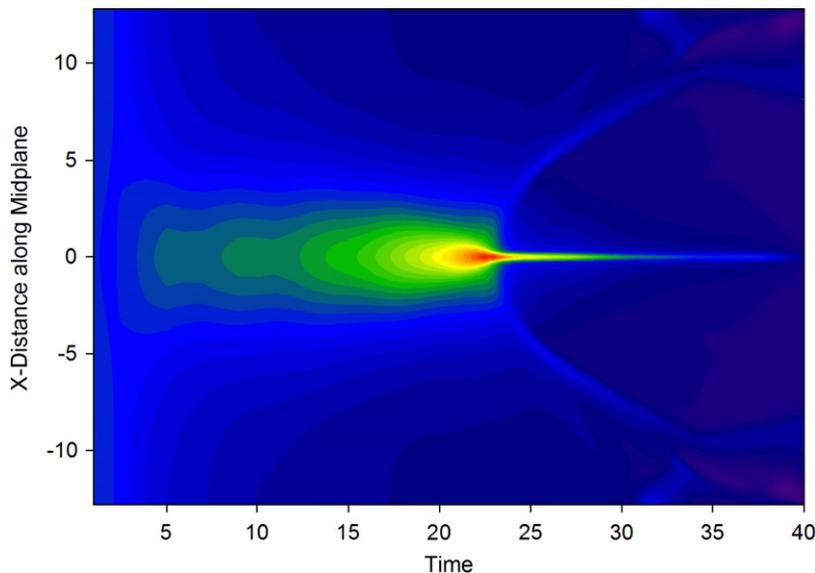

Fig. 6. Midplane Current density vs time. Vertical axis is current density along midplane $y = 0$, and horizontal axis is time. Note the abrupt transition at $t \sim 24$.
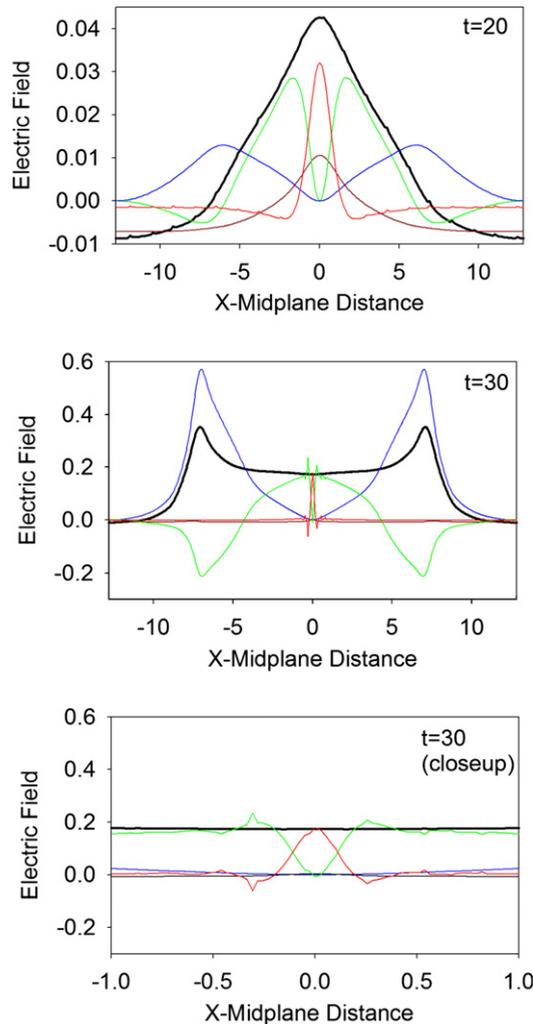
Fig. 7. Different components of the Electric Field. Solid black line is the total electric field. Green line is part due to $J \times B$ term, blue to the $V \times B$ term, dark red to the resistive term, and the bright red to the hyper-resistive term. Top figure is before transition, middle is after transition, and bottom is close-up of middle figure.

$$\hat{z} \cdot \vec{E} = \frac{1}{ne}\hat{z} \cdot \vec{J} \times \vec{B} - \hat{z} \cdot \vec{V} \times \vec{B} + \eta\hat{z} \cdot \vec{J} - C_H\eta h^2\nabla^2\hat{z} \cdot \vec{J} \qquad (10.3)$$

The terms in Eq. (10.3) are written in the order in which they occur when traversing down a vertical line in Fig. 7a (top) at the location $x = 10$. The top, bold curve is the total electric field. The next curves are the field due to the $J \times B$ term, the $V \times B$ term, the resistive term, and the hyper-resistive term. We can see from Fig. 7b (middle) that at time $t = 30$, after the transition, the $J \times B$ is the only significant contribution to the electric field in the vicinity of the x-point (central location), but that it must vanish exactly at the x-point since the magnetic field vanishes there ($B = 0$). In Fig. 7c (bottom), which is a blowup of Fig. 7b, we see that in the very near vicinity of the x-point, the term due to the hyper-resistivity becomes important. The scaling factor of h^2 was, in fact, chosen so that there would always be several triangular elements within this transition region. It has been shown previously that this leads to a globally convergent result in the limit as $1/N \sim h \to 0$ where the maximum reconnection rate and reconnected flux converge to a unique value [18].

Finally, we show in Fig. 8 some results comparing the series of calculation with everything else the same but different spatial resolutions (different number of elements). These graphs show both what stringent resolution
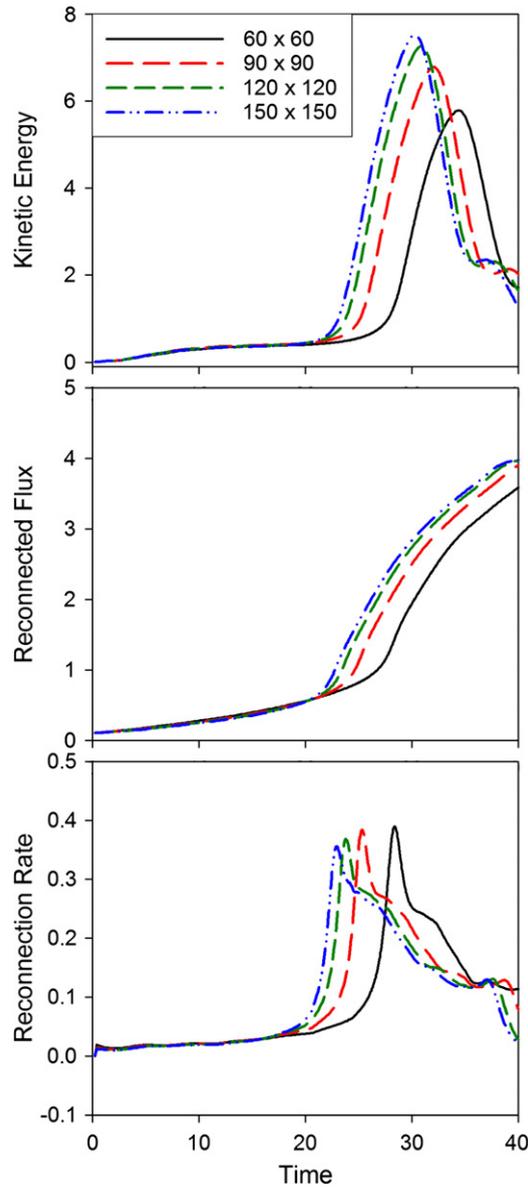
Fig. 8. Top figure is global kinetic energy vs time for four calculations with differing resolution, middle figure is the flux change at the midpoint vs time, and bottom graph is the time derivative of the middle curves. Reconnected Flux (middle curves) at time $t = 40$ is seen to be converging to a unique value.

requirements this problem has, and that the global quantities are converging, although slowly. We postulate that the slow convergence is due to the singular nature of the current sheet after the transition.

The time advance equations are not written in conservation form, although they should conserve energy as discussed following Eq. (2.3). We find that the numerical results conserve global energy to better than 1 part in 10^3 throughout the 120×120 calculation, and that this relative error decreases for the better resolved calculations.

11. Summary and future directions

We have described a method for solving a high-order set of partial differential equations providing a two-fluid description of a high temperature magnetized plasma in a relatively simple geometry and in 2D. The flux

function/potential representation of the vector velocity and magnetic fields leads to a representation in which the divergence of the magnetic field is intrinsically zero, and which allows accurate computation of nearly incompressible flow fields.

As discussed in [3], the technique should compare favorably with other finite element based methods in 2D. The fact that all the DOF are located at the nodes and are shared by all the surrounding triangles leads to a very compact representation. The C^1 continuity property allows computation with spatial operators containing up to fourth-order derivatives without introducing new auxiliary variables. A split semi-implicit method is used that breaks the full time advance into four sequential time advances, each involving smaller matrices. These features make feasible direct solution of the resulting sparse matrix equations, avoiding the slow convergence problems that would result if an iterative method were applied to these multiscale equations.

Illustrative examples are given of plane wave propagation, the computation of linear eigenmodes of a tilting cylinder, and a challenging problem in magnetic reconnection. Earlier studies have also demonstrated the applicability of this technique to the gravitational instability [13].

Work is presently underway to extend this work in several directions. It is being extended to cylindrical geometry in order to be applicable to an axisymmetric torus. An adaptive algorithm is being implemented to allow concentration of nodes in regions of high gradients. Three-dimensional extensions are being considered where the third dimension is represented by finite differences or by a spectral expansion. Indications are that the techniques demonstrated here form a powerful base that can be extended into more complex geometries.

Acknowledgements

Appendix A. Definitions of the operators

I. *Operators with 2 indices*:

$$A_{i,j}U_j \equiv \int\int v_i \nabla^2 U \, \mathrm{d}\xi \, \mathrm{d}\eta$$

$$B_{i,j}U_j \equiv \int\int v_i \nabla^4 U \, \mathrm{d}\xi \, \mathrm{d}\eta$$

$$D_{i,j}U_j \equiv \int\int v_i U \, \mathrm{d}\xi \, \mathrm{d}\eta$$

$$X^0_{i,j}N_j \equiv \int\int v_i n_x \, \mathrm{d}\xi \, \mathrm{d}\eta$$

$$Y^0_{i,j}N_j \equiv \int\int v_i n_y \, \mathrm{d}\xi \, \mathrm{d}\eta$$

II. *Operators with three indices*:

$$K_{i,j,k}\Psi_j U_k \equiv \int\int v_i[\psi, U]\mathrm{d}\xi \, \mathrm{d}\eta = -K_{i,k,j}\Psi_j U_k$$

$$K^1_{i,j,k}\Psi_k U_j \equiv \int\int v_i\psi U \mathrm{d}\xi \, \mathrm{d}\eta = K^1_{i,k,j}\Psi_k U_j$$

$$K^2_{i,j,k}N_k V_j \equiv \int\int (v_i n, V_z)\mathrm{d}\xi \, \mathrm{d}\eta$$

$$G_{i,j,k}\Psi_j U_k \equiv \int\int v_i[\nabla^2\psi, U]\mathrm{d}\xi\,\mathrm{d}\eta = -\int\int \nabla^2\psi[v_i, U]\mathrm{d}\xi\,\mathrm{d}\eta$$

$$G^2_{i,j,k}N_k\dot{U}_j \equiv -\int\int n(v_i, \dot{U})\mathrm{d}\xi\,\mathrm{d}\eta$$

$$G^3_{i,j,k}U_j N_k \equiv \int\int v_i\{-n\nabla^4 U - (n, \nabla^2 U)\}\mathrm{d}\xi\,\mathrm{d}\eta = -\int\int \nabla^2 U\nabla\cdot(n\nabla v_i)\mathrm{d}\xi\,\mathrm{d}\eta$$

$$G^4_{i,j,k}\Psi_j\Psi_k \equiv \int\int \nabla^2\psi(v_i, \psi)\mathrm{d}\xi\,\mathrm{d}\eta$$

$$G^5_{i,j,k}I_j I_k \equiv -\int\int v_i\tfrac{1}{2}\nabla^2 I^2 d\xi d\eta = \int\int I(I, v_i)\mathrm{d}\xi\,\mathrm{d}\eta$$

$$G^{6A}_{i,j,k}\dot{X}_j P_k \equiv -\int\int (v_i, (p, \dot{\chi}))\mathrm{d}\xi\,\mathrm{d}\eta$$

$$G^{6B}_{i,j,k}\dot{X}_j P_k \equiv \int\int p\nabla^2\dot{\chi}\nabla^2 v_i\mathrm{d}\xi\,\mathrm{d}\eta$$

$$G^7_{i,j,k}\dot{U}_j P_k \equiv -\int\int (v_i, [p, \dot{U}])\mathrm{d}\xi\,\mathrm{d}\eta$$

$$G^{12}_{i,j,k}I_j I_k \equiv \int\int v_i(I_{xx}^2 + I_{yy}^2 + 2I_{xy}^2)\mathrm{d}\xi\,\mathrm{d}\eta$$

$$G^{13}_{i,j,k}E_k P_j \equiv \int\int v_i\nabla^4(pE)d\xi d\eta = \int\int \nabla^2 v_i\nabla^2(pE)\mathrm{d}\xi\,\mathrm{d}\eta$$

$$G^{14}_{i,j,k}U_j U_k \equiv \int\int v_i\{(U_{yy} - U_{xx})^2 + 4U_{xy}^2\}\mathrm{d}\xi\,\mathrm{d}\eta$$

$$G^{15}_{i,j,k}X_j X_k \equiv \int\int v_i(4\chi_{xy}^2 - 4\chi_{xx}\chi_{yy} + 2|\nabla^2\chi|^2)\mathrm{d}\xi\,\mathrm{d}\eta$$

$$G^{16}_{i,j,k}U_j X_k \equiv \int\int v_i 4\{U_{xy}(\chi_{xx} - \chi_{yy}) + \chi_{xy}(U_{yy} - U_{xx})\}\mathrm{d}\xi\,\mathrm{d}\eta$$

$$G^{17}_{i,j,k}X_j X_k \equiv \int\int v_i|\nabla^2\chi|^2\mathrm{d}\xi\,\mathrm{d}\eta$$

$$H^3_{i,j,k}S_{\psi k}\Psi_j \equiv \int\int \{-J(v_i, S_\psi) - \nabla^2 S_\psi(v_i, \psi)\}\mathrm{d}\xi\,\mathrm{d}\eta$$

$$H^5_{i,j,k}S_{Ik}I_j \equiv \int\int \{-I(v_i, S_I) - S_I(I, v_i)\}\mathrm{d}\xi\,\mathrm{d}\eta$$

$$X^1_{i,j,k}N_k U_j \equiv \int\int v_i[n, U]_x\mathrm{d}\xi\,\mathrm{d}\eta$$

$$X^2_{i,j,k}N_k X_j \equiv \int\int v_i[(n, \chi) + n\nabla^2\chi]_x\mathrm{d}\xi\,\mathrm{d}\eta$$

$$Y^1_{i,j,k}N_k U_j \equiv \int\int v_i[n, U]_y\mathrm{d}\xi\,\mathrm{d}\eta$$

$$Y^2_{i,j,k}N_k X_j \equiv \int\int v_i[(n, \chi) + n\nabla^2\chi]_y\mathrm{d}\xi\,\mathrm{d}\eta$$

III. *Operators with four indices*:

$$V^1_{i,j,k,l}N_l U_k U_j = V^2_{i,k,j,l}N_l U_k U_j \equiv \int\int \{-n\nabla^2 U[v_i, U] + \tfrac{1}{2}n[v_i, (U, U)]\}\mathrm{d}\eta\,\mathrm{d}\xi$$

$$V^3_{i,j,k,l}N_l X_k U_j = V^4_{i,k,j,l}N_l X_k U_j \equiv \int\int v_i\{-n\nabla^2 U(v_i, \chi) + [n, v_i][\chi, U]\}\mathrm{d}\eta\,\mathrm{d}\xi$$

$$V^5_{i,j,k,l}N_l X_k X_j = V^6_{i,k,j,l}N_l X_k X_j \equiv -\tfrac{1}{2}\int\int v_i[n, (\chi, \chi)]\mathrm{d}\eta\,\mathrm{d}\xi$$

$$V^7_{i,j,k,l}N_lU_kV_{zj} = V^8_{i,k,j,l}N_lU_kV_{zj} \equiv \int\int v_i n[V_z, U]\mathrm{d}\xi\,\mathrm{d}\eta$$

$$V^9_{i,j,k,l}N_lX_kV_{zj} = V^{10}_{i,k,j,l}N_lX_kV_{zj} \equiv \int\int v_i n(V_z, \chi)\mathrm{d}\xi\,\mathrm{d}\eta$$

$$V^{11}_{i,j,k,l}N_lU_kX_j = V^{12}_{i,k,j,l}N_lU_kX_j \equiv \int\int \{-n\nabla^2 U[v_i, \chi] - n(v_i, [\chi, U])\}\mathrm{d}\eta\,\mathrm{d}\xi$$

$$V^{13}_{i,j,k,l}N_lX_kX_j = V^{14}_{i,k,j,l}N_lX_kX_j \equiv -\tfrac{1}{2}\int\int n(v_i, (\chi, \chi))\mathrm{d}\eta\,\mathrm{d}\xi$$

$$V^{15}_{i,j,k,l}N_lU_kU_j = V^{16}_{i,k,j,l}N_lU_kU_j \equiv \int\int \{n\nabla^2 U(v_i, U) - \tfrac{1}{2}n(v_i, (U, U))\}\mathrm{d}\eta\,\mathrm{d}\xi$$

$$C^1_{i,j,k,l}\Psi_k\Psi_l\dot{U}_j \equiv \nabla^2\psi[[\psi, \dot{U}], v_i] + ([\psi, \dot{U}], [v_i, \psi])$$

$$C^3_{i,j,k,l}\Psi_k\Psi_l\dot{X}_j \equiv \nabla^2\psi[(\psi, \dot{\chi}), v_i] + ((\psi, \dot{\chi}), [v_i, \psi])$$

$$C^5_{i,j,k,l}I_l\psi_k\dot{U}_j = -[\psi, \dot{U}][v_i, I] + [I, \dot{U}][v_i, \psi]$$

$$C^7_{i,j,k,l}I_l\psi_k\dot{X}_j = -(\psi, \dot{\chi})[v_i, I] + (I, \dot{\chi})[v_i, \psi] + I\nabla^2\dot{\chi}[v_i, \psi]$$

$$C^9_{i,j,k,l}\psi_l\psi_k\dot{V}_j = -[\psi, V_j][\psi, v_i]$$

$$C^{11}_{i,j,k,l}\Psi_l\Psi_k\dot{U}_j = -((v_i, \psi), [\psi, \dot{U}]) + \nabla^2\psi(v_i, [\psi, \dot{U}])$$

$$C^{13}_{i,j,k,l}\dot{X}_j\Psi_k\Psi_l = -((v_i, \psi), (\psi, \dot{\chi})) + \nabla^2\psi(v_i, (\psi, \chi))$$

$$C^{15}_{i,j,k,l}\dot{V}_j\Psi_kI_l = -I[\psi, \dot{V}]\nabla^2 v_i$$

$$C^{17}_{i,j,k,l}\dot{X}_jI_kI_l = -I[I\nabla^2\dot{\chi} + (I, \dot{\chi})]\nabla^2 v_i$$

$$U^1_{i,j,k,l}E_l\Psi_j\Psi_k = U^2_{i,k,j,l}E_l\Psi_j\Psi_k = -\int\int \nabla^2\Psi E[v_i, \Psi]\mathrm{d}\xi\,\mathrm{d}\eta$$

$$U^3_{i,j,k,l}E_l\Psi_jI_k = U^4_{i,k,j,l}E_l\Psi_jI_k = \int\int v_i E[\Psi, I]\mathrm{d}\xi\,\mathrm{d}\eta$$

$$U^5_{i,j,k,l}E_lP_{ej}I_k = U^6_{i,k,j,l}E_lP_{ej}I_k = \int\int v_iP_e[E, I]\mathrm{d}\xi\,\mathrm{d}\eta$$

Appendix B. Computation of the operators

Each of the scalar variables is expanded within each element as a sum over the 18 basis functions, for example as given in Eq. (3.2). Each basis function is a quintic polynomial in the local triangle coordinates given in [3], i.e.

$$v_j \equiv \sum_{i=1}^{20} g_{i,j}\xi^{m_i}\eta^{n_i} \tag{B.1}$$

To obtain the form of the operators, we expand all variables in the polynomial representation and apply the operation and integrations in the local coordinates. Thus, for example,

$$A_{i,j}\Phi_j \equiv \int\int v_i(\xi, \eta)\nabla^2\phi(\xi, \eta)\mathrm{d}\xi\,\mathrm{d}\eta = -\int\int \nabla v_i(\xi, \eta)\cdot\nabla\phi(\xi, \eta)\mathrm{d}\xi\,\mathrm{d}\eta$$

$$= -\sum_{p=1}^{20}\sum_{q=1}^{20}\sum_{j=1}^{18} g_{p,i}g_{q,j}\left[m_pm_q\int\int \xi^{m_p+m_q-2}\eta^{n_p+n_q}\mathrm{d}\xi\,\mathrm{d}\eta + n_pn_q\int\int \xi^{m_p+m_q}\eta^{n_p+n_q-2}\mathrm{d}\xi\,\mathrm{d}\eta\right] \tag{B.2}$$

where $g_{p,i}$ is the geometry matrix defined in [3] and the integrals over the triangle are evaluated in closed form. In the concise notation that follows, we will write this as

$$A_{i,j}\Phi_j = -[m_p m_q F(-2,0) + n_p n_q F(0,-2)]. \tag{B.3}$$

The summations, the multiplication by the appropriate geometry matrices, and the integrals involving the m_i and n_i are implied. The other operators are computed similarly, using the same notation.

$$B_{i,j} = m_p(m_p - 1)m_q(m_q - 1) \times F(-4,0) + n_p(n_p - 1)n_q(n_q - 1) \times F(0,-4)$$
$$\quad + [m_p(m_p - 1)n_q(n_q - 1) + m_q(m_q - 1)n_p(n_p - 1)] \times F(-2,-2)$$

$$D_{i,j} = F(0,0)$$

$$X^0_{i,j} = \cos\theta m_q F(-1,0) - \sin\theta n_q F(0,-1)$$

$$Y^0_{i,j} = \sin\theta m_q F(-1,0) + \cos\theta n_q F(0,-1)$$

$$K_{i,j,k} = (m_q n_r - m_r n_q)F(-1,-1)$$

$$K^1_{i,j,k} = F(0,0)$$

$$K^2_{i,j,k} = (m_p + m_r)m_q F(-2,0) + (n_p + n_r)n_q F(-2,0)$$

$$G_{i,j,k} = -(m_p n_r - m_r n_p)[m_q(m_q - 1)F(-3,-1) + n_q(n_q - 1)F(-1,-3)]$$

$$G^2_{i,j,k} = -[m_p m_q F(-2,0) + n_p n_q F(0,-2)]$$

$$G^3_{i,j,k} = [m_p m_q(m_q - 1)(m_p + m_r - 1)]F(-4,0) + [n_p n_q(n_q - 1)(n_p + n_r - 1)]F(0,-4)$$
$$\quad + [n_p m_q(m_q - 1)(n_p + n_r - 1) + m_p n_q(n_q - 1)(m_p + m_r - 1)]F(-2,-2)$$

$$G^4_{i,j,k} = m_q(m_q - 1)m_p m_r F(-4,0) + n_q(n_q - 1)n_p n_r F(0,-4)$$
$$\quad + [m_q(m_q - 1)n_p n_r + n_q(n_q - 1)m_p m_r]F(-2,-2)$$

$$G^5_{i,j,k} = m_p m_r F(-2,0) + n_p n_r F(0,-2)$$

$$G^6_{i,j,k} = [m_p m_q\{-m_r(m_r + m_q - 2) + \gamma(m_q - 1)(m_p - 1)\}]F(-4,0)$$
$$\quad + [+m_p n_q\{-n_r(m_r + m_q) + \gamma(n_q - 1)(m_p - 1)\} + n_p m_q\{-m_r(n_r + n_q) + \gamma(m_q - 1)(n_p - 1)\}]F(-2,-2)$$
$$\quad + [n_p n_q\{-n_r(n_r + n_q - 2) + \gamma(n_q - 1)(n_p - 1)\}]F(0,-4)$$

$$G^7_{i,j,k} = -(m_r n_q - m_q n_r)[m_p(m_r + m_q - 1) \times F(-3,-1) + n_p(n_r + n_q - 1) \times F(-1,-3)]$$

$$G^{12}_{i,j,k} = m_q(m_q - 1)m_r(m_r - 1) \times F(-4,0) + 2m_q m_r n_q n_r \times F(-2,-2)$$
$$\quad + n_q(n_q - 1)n_r(n_r - 1) \times F(0,-4)$$

$$G^{13}_{i,j,k} = (m_q + m_r)(m_q + m_r - 1)m_p(m_p - 1) \times F(-4,0)$$
$$\quad + \begin{bmatrix}(m_q + m_r)(m_q + m_r - 1)n_p(n_p - 1) \\ +(n_q + n_r)(n_q + n_r - 1)m_p(m_p - 1)\end{bmatrix} \times F(-2,-2)$$
$$\quad + (n_q + n_r)(n_q + n_r - 1)n_p(n_p - 1) \times F(0,-4)$$

$$G^{14}_{i,j,k} = m_q(m_q - 1)m_r(m_r - 1)F(-4,0) + n_q(n_q - 1)n_r(n_r - 1)F(0,-4)$$
$$\quad + [-n_q(n_q - 1)m_r(m_r - 1) - m_q(m_q - 1)n_r(n_r - 1) + 4m_q n_q m_r n_r]F(-2,-2)$$

$$G^{15}_{i,j,k} = 2[m_q(m_q - 1)m_r(m_r - 1)F(-4,0) + n_q(n_q - 1)n_r(n_r - 1)F(0,-4) + 2m_q n_q m_r n_r F(-2,-2)]$$

$$G^{16}_{i,j,k} = 4m_q m_r[n_q(m_r - 1) - n_r(m_q - 1)]F(-3,-1) - 4n_q n_r[m_q(n_r - 1) - m_r(n_q - 1)]F(-1,-3)$$

$$G^{17}_{i,j,k} = m_q(m_q - 1)m_r(m_r - 1)F(-4,0) + n_q(n_q - 1)n_r(n_r - 1)F(0,-4)$$
$$\quad + [m_q(m_q - 1)n_r(n_r - 1) + n_q(n_q - 1)m_r(m_r - 1)]F(-2,-2)$$

$$H^3_{i,j,k} = -m_p m_q m_r(m_r + m_q - 2)F(-4,0) - n_p n_q n_r(n_r + n_q - 2)F(0,-4)$$
$$\quad - [m_q n_r(m_p(n_r - 1) + n_p(m_q - 1)) + n_q m_r(n_p(m_r - 1) + m_p(n_q - 1))]F(-2,-2)$$

$$H^5_{i,j,k} = -m_p(m_r + m_q)F(-2,0) - n_p(n_r + n_q)F(0,-2)$$

$$X^1_{i,j,k} = (m_q n_r - m_r n_q)[m_p \cos\theta F(-2,-1) + n_p \sin\theta F(-1,-2)]$$

$$X^2_{i,j,k} = -m_q(m_r + m_q - 1)[m_p \cos\theta F(-3,0) - n_p \sin\theta F(-2,-1)]$$
$$- n_q(n_r + n_q - 1)[m_p \cos\theta F(-1,-2) - n_p \sin\theta F(0,-3)]$$

$$Y^1_{i,j,k} = (m_q n_r - m_r n_q)[m_p \sin\theta F(-2,-1) + n_p \cos\theta F(-1,-2)]$$

$$Y^2_{i,j,k} = -m_q(m_r + m_q - 1)[m_p \sin\theta F(-3,0) + n_p \cos\theta F(-2,-1)]$$
$$- n_q(n_r + n_q - 1)[m_p \sin\theta F(-1,-2) + n_p \cos\theta F(0,-3)]$$

$$V^1_{i,j,k,l} = \begin{bmatrix} m_q\{m_r[(m_q-1)(n_s+n_p) - n_q m_s] - n_r m_p(m_q-1)\} \times F(-3,-1) \\ +n_q\{m_r n_p(n_q-1) + n_r[m_q n_s - (n_q-1)(m_s+m_p)]\} \times F(-1,-3) \end{bmatrix}$$

$$V^3_{i,j,k,l} = \begin{Bmatrix} [-m_r m_p m_q(m_q-1)]F(-4,0) \\ + \begin{Bmatrix} m_r n_q[(m_r+m_q-1)n_s - (n_q-1)(m_s+m_p) - m_s n_r] \\ +n_r m_q[(n_r+n_q-1)m_s - (m_q-1)(n_s+n_p) - n_s m_r] \end{Bmatrix} F(-2,-2) \\ +[-n_r n_p n_q(n_q-1)]F(0,-4) \end{Bmatrix}$$

$$V^5_{i,j,k,l} = \tfrac{1}{2}(m_s n_p - m_p n_s)[m_r m_q F(-3,-1) + n_r n_q F(-1,-3)]$$

$$V^7_{i,j,k,l} = [m_q n_r - m_r n_q]F(-1,-1)$$

$$V^9_{i,j,k,l} = [m_q m_r F(-2,0) + n_q n_r F(0,-2)]$$

$$V^{11}_{i,j,k,l} = \begin{Bmatrix} -[(m_p n_q - m_q n_p)m_r(m_r-1) + (m_q n_r - m_r n_q)m_p(m_q+m_r-1)]F(-3,-1) \\ -[(m_p n_q - m_q n_p)n_r(n_r-1) + (m_q n_r - m_r n_q)n_p(n_q+n_r-1)]F(-1,-3) \end{Bmatrix}$$

$$V^{13}_{i,j,k,l} = \begin{Bmatrix} \tfrac{1}{2}m_p m_q m_r(m_p+m_s-1)F(-4,0) \\ +\tfrac{1}{2}\begin{bmatrix} m_p n_q n_r(m_p+m_s-1) \\ +n_p m_q m_r(n_p+n_s-1) \end{bmatrix} F(-2,-2) \\ +\tfrac{1}{2}n_p n_q n_r(n_p+n_s-1)F(0,-4) \end{Bmatrix}$$

$$V^{15}_{i,j,k,l} = \begin{Bmatrix} [-\tfrac{1}{2}m_p m_r m_q(m_r-m_q)]F(-4,0) \\ + \begin{bmatrix} m_p m_r n_q(n_q-1) + n_p n_r m_q(m_q-1) \\ -\tfrac{1}{2}m_p n_r n_q(m_r+m_q) - \tfrac{1}{2}n_p m_r m_q(n_r+n_q) \end{bmatrix} F(-2,-2) \\ +[-\tfrac{1}{2}n_p n_r n_q(n_r-n_q)]F(0,-4) \end{Bmatrix}$$

$$C^1_{i,j,k,l} = (m_s n_q - m_q n_s) \times \begin{Bmatrix} \begin{bmatrix} m_r(m_r-1)[(m_s+m_q-1)n_p - m_p(n_s+n_q-1)] \\ +(m_p n_r - m_r n_p)(m_s+m_q-1)(m_p+m_r-1) \end{bmatrix} F(-4,-2) \\ + \begin{bmatrix} n_r(n_r-1)[(m_s+m_q-1)n_p - m_p(n_s+n_q-1)] \\ +(m_p n_r - m_r n_p)(n_s+n_q-1)(n_p+n_r-1) \end{bmatrix} F(-2,-4) \end{Bmatrix}$$

$$C^3_{i,j,k,l} = m_r m_q \begin{Bmatrix} (m_p n_s - m_s n_p)[(m_r+m_q-2)(m_p+m_s-1)] \\ +m_s(m_s-1)[(m_r+m_q-2)n_p - m_p(n_r+n_q)] \end{Bmatrix} F(-5,-1)$$
$$+ \begin{Bmatrix} m_r m_q \begin{pmatrix} (m_p n_s - m_s n_p)[(n_r+n_q)(n_p+n_s-1)] \\ +n_s(n_s-1)[(m_r+m_q-2)n_p - m_p(n_r+n_q)] \end{pmatrix} \\ +n_r n_q \begin{pmatrix} (m_p n_s - m_s n_p)[(m_r+m_q)(m_p+m_s-1)] \\ +m_s(m_s-1)[(m_r+m_q)n_p - m_p(n_r+n_q-2)] \end{pmatrix} \end{Bmatrix} F(-3,-3)$$
$$+ n_r n_q \begin{Bmatrix} (m_p n_s - m_s n_p)[(n_r+n_q-2)(n_p+n_s-1)] \\ +n_s(n_s-1)[(m_r+m_q)n_p - m_p(n_r+n_q-2)] \end{Bmatrix} F(-1,-5)$$

$$C^5_{i,j,k,l} = [-(m_r n_q - m_q n_r)(m_p n_s - m_s n_p) + (m_s n_q - m_q n_s)(m_p n_r - m_r n_p)]F(-2,-2)$$

$$C^7_{i,j,k,l} = -m_q\{m_r(m_p n_s - m_s n_p) + (m_r n_p - m_p n_r)[m_s + m_q - 1]\}F(-3,-1)$$
$$- n_q\{n_r(m_p n_s - m_s n_p) + (m_r n_p - m_p n_r)[n_s + n_q - 1]\}F(-1,-3)$$

$$C^9_{i,j,k,l} = -(m_r n_p - m_p n_r)(m_s n_q - m_q n_s)F(-2,-2)$$

$$C_{i,j,k,l}^{11} = -(m_s n_q - m_q n_s) \times \begin{bmatrix} m_p m_r (m_p - 1)(m_s + m_q - 1)F(-5,-1) \\ \begin{bmatrix} (n_p n_r(m_p + m_r) - m_p n_r(n_r - 1))(m_s + m_q - 1) \\ +(m_p m_r(n_p + n_r) - n_p m_r(m_r - 1))(n_s + n_q - 1) \end{bmatrix} F(-3,-3) \\ n_p n_r(n_p - 1)(n_s + n_q - 1)F(-1,-5) \end{bmatrix}$$

$$C_{i,j,k,l}^{13} = \begin{Bmatrix} -(m_p - 1)m_s m_p m_r m_q(m_r + m_q - 2)F(-6,0) \\ +\begin{Bmatrix} [n_p(m_s - 1) - m_p(n_p + n_s)]m_s m_r m_q(n_r + n_q) \\ +[(n_s - n_p - 1)m_p - n_p m_s]n_s m_r m_q(m_r + m_q - 2) \\ +(1 - m_p)n_r n_q m_p m_s(m_r + m_q) \end{Bmatrix} F(-4,-2) \\ +\begin{Bmatrix} [m_p(n_s - 1) - n_p(m_p + m_s)]n_s n_r n_q(m_r + m_q) \\ +[(m_s - m_p - 1)n_p - m_p n_s]m_s n_r n_q(n_r + n_q - 2) \\ +(1 - n_p)m_r m_q n_p n_s(n_r + n_q) \end{Bmatrix} F(-2,-4) \\ -(n_p - 1)n_s n_p n_r n_q(n_r + n_q - 2)F(0,-6) \end{Bmatrix}$$

$$C_{i,j,k,l}^{15} = -(m_r n_q - m_q n_r)[m_p(m_p - 1)F(-3,-1) + n_p(n_p - 1)F(-1,-3)]$$

$$C_{i,j,k,l}^{17} = -m_p m_q[(m_q + m_s - 1)(m_p - 1)]F(-4,0) + n_p n_q[(n_q + n_s - 1)(n_p - 1)]F(0,-4)$$
$$+ \{n_p m_q[(m_q + m_s - 1)(n_p - 1)] + m_p n_q[(n_q + n_s - 1)(m_p - 1)]\}F(-2,-2)$$

$$U_{i,j,k,l}^{1} = -[m_p n_r - m_r n_p] \times [m_q(m_q - 1)F(-3,-1) + n_q(n_q - 1)F(-1,-3)]$$

$$U_{i,j,k,l}^{3} = (m_q n_r - m_r n_q)F(-1,-1)$$

$$U_{i,j,k,l}^{5} = (m_s n_r - m_r n_s)F(-1,-1)$$

Appendix C. The implicit time advance for a simple wave equation

Here we apply the time advance used in the paper to a simple wave equation to clarify the derivation, stability properties, and accuracy. Consider a wave equation written as two first-order equations:

$$\frac{\partial u}{\partial t} = c\frac{\partial v}{\partial x}$$
$$\frac{\partial v}{\partial t} = c\frac{\partial u}{\partial x} \tag{C.1}$$

Rewrite this system, centering the time derivatives at time cycle $n + 1/2$, and Taylor expanding the space derivatives forward in time about time n:

$$\frac{\partial u}{\partial t} = c\frac{\partial}{\partial x}\left[v^n + \theta\delta t\frac{\partial v}{\partial t}\right]$$
$$\frac{\partial v}{\partial t} = c\frac{\partial}{\partial x}\left[u^n + \theta\delta t\frac{\partial u}{\partial t}\right] \tag{C.2}$$

Or, upon substitution of the second equation into the first:

$$\frac{\partial u}{\partial t} = c\frac{\partial}{\partial x}\left[v^n + \theta\delta t\left(c\frac{\partial}{\partial x}\left[u^n + \theta\delta t\frac{\partial u}{\partial t}\right]\right)\right]$$
$$\frac{\partial v}{\partial t} = c\frac{\partial}{\partial x}\left[u^n + \theta\delta t\frac{\partial u}{\partial t}\right] \tag{C.3}$$

Expanding the time-centered time derivatives as $\delta t\partial u/\partial t = u^{n+1} - u^n$, and rearranging, Eq. (C.3) becomes:

$$\left[1 - \theta^2(\delta t)^2 c^2\frac{\partial^2}{\partial x^2}\right]u^{n+1} = \left[1 + \theta(1 - \theta)(\delta t)^2 c^2\frac{\partial^2}{\partial x^2}\right]u^n + \delta t c\frac{\partial}{\partial x}v^n$$

$$v^{n+1} = v^n + \delta t c \left[\theta \frac{\partial}{\partial x} u^{n+1} + (1-\theta) \frac{\partial}{\partial x} u^n \right]$$

If we evaluate the spatial derivatives using centered differences or finite elements, the system (C.4) is second-order accurate in time for $\theta = 1/2$ and unconditionally stable for $\theta \geqslant 1/2$. Note that the two equations in (C.4) can be solved sequentially, so that the implicit system only involves one variable. The first equation in (C.3) is the analogue of Eq. (4.5), and the first equation in (C.4) is the analogue of Eq. (4.7).

References

[1] R. Gruber, J. Rappaz, Finite Element Methods in Linear Ideal MHD, Springer, 1985.
[2] D. Schnack, D.C. Barnes, D.P. Brennan, et al., Computational modeling of fully ionized magnetized plasmas using the fluid approximation, Phys. Plasma 13 (2006) (Art. No. 058103).
[3] S.C. Jardin, A triangular finite element with first-derivative continuity applied to fusion MHD applications, J. Comput. Phys 200 (2004) 133.
[4] S.C. Jardin, J.A. Breslau, Implicit solution of the four-field extended-magnetohydrodynamic equations using high-order high-continuity finite elements, Phys. Plasma 12 (2005) 056101.
[5] C.R. Sovinec, A.H. Glasser, G.A. Gianakon, et al., J. Comput. Phys. 195 (2004) 355.
[6] L. Chacon, D.A. Knoll, J.M. Finn, Implicit, nonlinear reduced resistive MHD nonlinear solver, J. Comput. Phys 178 (1) (2002) 15–36.
[7] L. Chacon, D.A. Knoll, A 2D high-beta Hall MHD implicit nonlinear solver, J. Comput. Phys 188 (2) (2003) 573–592.
[8] A.H. Glasser, X.Z. Tang, The SEL macroscopic modeling code, Comp. Phys. Commun. 164 (2004) 237.
[9] G. Strang, G. Fix, An Analysis of the Finite Element Method, Prentice-Hall, NJ, 1973.
[10] O.C. Zienkiewicz, The Finite Element Method, third ed., McGraw-Hill, London, 1977.
[11] M. Zlamal, Some recent advances in the mathematics of finite elements, in: J.R. Whiteman (Ed.), The Mathematics of Finite Elements and Applications, Academic Press, 1973, pp. 59–79.
[12] L.D. Landau, E.M. Lifschitz, Fluid Mechanics, Addison-Wesley, Reading, MA, 1959.
[13] N. Ferraro, S.C. Jardin, Finite element implementation of Braginskii's gyroviscous stress with application to the gravitational instability, Phys. Plasmas 13 (092101) (2006).
[14] W. Park, E.V. Belova, G.Y. Fu, et al., Phys. Plasmas 6 (1999) 1796–1803 (Part 2).
[15] I.N. Molchanov, L.D. Nikolenko, On an approach to Integrating Boundary Problems with a non-unique solution, Inform. Process. Lett. 1 (1972) 168–172.
[16] R.L. Richard, R.D. Sydora, M. Ashour-Abdalla, Magnetic reconnection driven by current repulsion, Phys. Fluids B 2 (1990) 488.
[17] J. Birn, J.F. Drake, M.A. Shay, et al., J. Geophys. Res. [Space Phys.] 106 (2001) 3715.
[18] J. Breslau, S.C. Jardin, Phys. Plasmas 10 (2003) 1291.
[19] J.W. Demmel, J.R. Gilbert, Y.S. Li, SUPERLU: Users Guide, U.C. Berkeley, 2003.
[20] S.I. Braginskii, Transport processes in a plasma, Reviews of Modern Physics, vol. 205, Consultants Bureau, New York, 1965.
[21] E.J. Caramana, J. Comput. Phys. 96 (1991) 484–493.
[22] B. Scott, Phys. Plasmas 12 (2005) 102307.